Copy
RM L55F08

NACA RM L55F08

NACA

RESEARCH MEMORANDUM

LATERAL STABILITY AND CONTROL MEASUREMENTS OF A FIGHTER-TYPE AIRPLANE WITH A LOW-ASPECT-RATIO UNSWEPT WING AND A TEE-TAIL

By Donald D. Arabian and James W. Schmeer

Langley Aeronautical Laboratory
Langley Field, Va.

NATIONAL ADVISORY COMMITTEE
FOR AERONAUTICS

WASHINGTON
June 12, 1956
Declassified July 28, 1960

NACA RM L55F08

NATIONAL ADVISORY COMMITTEE FOR AERONAUTICS

RESEARCH MEMORANDUM

LATERAL STABILITY AND CONTROL MEASUREMENTS OF A FIGHTER-TYPE AIRPLANE WITH A LOW-ASPECT-RATIO UNSWEPT WING AND A TEE-TAIL

By Donald D. Arabian and James W. Schmeer

SUMMARY

An investigation of the lateral stability and control effectiveness of a 0.0858-scale model of a fighter-type airplane model has been conducted in the Langley 16-foot transonic tunnel. The model has a low-aspect-ratio, 3.4-percent-thick wing with negative dihedral. The horizontal tail is located on top of the vertical tail.

The investigation was made through a Mach number range of 0.80 to 1.06 at sideslip angles of -5° to 5° and angles of attack from 0° to 16°. The control effectiveness of the aileron, rudder, and yaw damper were determined through the Mach number and angle-of-attack range.

The results of the investigation indicated that the directional stability derivative C_{n_β} was stable and that positive effective dihedral existed throughout the lift-coefficient range and Mach number range tested.

The total aileron effectiveness, which in general produced favorable yaw with rolling moment, remained fairly constant for lift coefficients up to about 0.8 for the Mach number range tested. Yawing-moment effectiveness of the rudder changed little through the Mach number range. However, the yaw damper effectiveness decreased about 50 percent at the intermediate test Mach numbers.

INTRODUCTION

Flight at supersonic speeds has forced the design trend for fighter-type airplanes toward thin wings of low aspect ratio. At the present time, there is little information on the lateral stability characteristics of airplanes with this type wing, especially at the transonic

speeds. Of general interest, therefore, are the results of an investigation conducted in the Langley 16-foot transonic tunnel of a fighter-type model employing a straight wing, 3.4 percent thick, having an aspect ratio of 2.5, and a taper ratio of 0.385.

The results of the investigation of the static-lateral stability and control characteristics of the model, including the effects of the model components, are presented in this paper. Longitudinal and lateral experimental data for a comparable model at subsonic and supersonic speeds are available in references 1 and 2.

Data were obtained through a Mach number range of 0.80 to 1.06 at an average Reynolds number of about 3×10^6. At zero angle of attack, tests were run through a range of sideslip angle from -5° to 5°. At 0° and -5° of sideslip, the angle of attack was varied from 0° to 16°. Rudder and damper effectiveness was determined for a range of sideslip angle while the aileron effectiveness was determined for a range of angle of attack.

SYMBOLS

C_L lift coefficient, $\frac{\text{Lift}}{qS}$

C_n yawing-moment coefficient, $\frac{\text{Yawing moment}}{qSb}$

C_l rolling-moment coefficient, $\frac{\text{Rolling moment}}{qSb}$

C_Y lateral-force coefficient, $\frac{\text{Lateral force}}{qS}$

C_{l_β} rate of change of rolling-moment coefficient with angle of sideslip, per deg, $\frac{dC_l}{d\beta}$

C_{Y_β} rate of change of lateral-force coefficient with angle of sideslip, per deg, $\frac{dC_Y}{d\beta}$

C_{n_β} rate of change of yawing-moment coefficient with angle of sideslip, per deg, $\frac{dC_n}{d\beta}$

C_{L_α} lift-curve slope, per deg, $\frac{dC_L}{d\alpha}$

$C_{n_{\delta_d}}$ damper effectiveness, per deg, $\frac{dC_n}{d\delta_d}$

$C_{n_{\delta_r}}$ rudder effectiveness, per deg, $\frac{dC_n}{d\delta_r}$

$C_{l_{\delta_a}}$ aileron effectiveness, per deg, $\frac{dC_l}{d\delta_a}$

M Mach number

q free-stream dynamic pressure, lb/ft^2

S wing area, ft^2

b wing span, ft

α model angle of attack, deg (measured with respect to the fuselage reference)

β sideslip angle, deg

Γ dihedral angle, deg

δ_r rudder deflection, deg (positive trailing edge left)

δ_d yaw damper deflection, deg (positive trailing edge left)

δ_a aileron deflection, deg (positive trailing edge down)

MODEL AND APPARATUS

The tests were conducted in the Langley 16-foot transonic tunnel which is described in reference 3. The model was constructed of aluminum and steel and was mounted on the tunnel sting-support system through a six-component strain-gage balance. A three-view drawing of the model is shown in figure 1, and principal model dimensions are listed in table I. A modification to the fuselage permitted evaluation of the effect of internal flow on the data. This modification, termed a "modified afterbody" consisted of a short section attached to the under part of the fuselage to allow the internal flow to exhaust beneath the sting.

Photographs of the model with and without the modification are presented in figure 2.

CONFIGURATIONS AND TEST RANGE

A detailed list of configurations tested including the range of angle of sideslip and angle of attack is presented in table II. All the configurations were tested through a Mach number range of 0.80 to 1.06 at Reynolds numbers of about 2.8×10^6 to 3.3×10^6.

REDUCTION OF DATA

The force and moment data were corrected for weight tares and adjusted for free-stream static pressure at the model base. The effects of tunnel-wall reflected disturbances and of sting interference on the lateral characteristics have not been evaluated for this model in the 16-foot tunnel but are believed to be small.

The coefficients are referred to the stability axis system with the origin on the center line of the model at an axial location corresponding to the 0.25 mean aerodynamic chord. (See fig. 3.) Both the angle of attack and the angle of sideslip as presented in the report have been adjusted for stream angularity and for model deflection due to load and are believed correct within $\pm 0.1^\circ$. The estimated accuracy of the data is as follows:

C_l	± 0.002
C_n	± 0.002
C_L	± 0.005
C_Y	± 0.005

RESULTS

The results of the investigation are presented in the following figures:

DISCUSSION

Lateral Characteristics at Zero Angle of Attack

Effect of modified afterbody and internal flow.- The effect of the modified afterbody with and without internal flow on the lateral characteristics is shown for the tail-off configuration in figure 5 and for the complete model in figure 6. The addition of the modified afterbody increased the stability while the mass flow tended to decrease the stability toward that of the unmodified model. All subsequent data and discussion thereof will be for the model with internal flow. In these figures and several that follow, the data points have been omitted in the interest of clarity; however, the curves in each case have been faired through each data point.

Yawing moment and lateral force due to sideslip.- The variation of yawing moment with angle of sideslip is linear through the Mach number range for the wing-body configuration (fig. 7). With the addition of the vertical tail, nonlinearities appear which may be attributed to the effects on the vertical tail of the nonlinear induced cross flow of the fuselage and the asymmetric loading of the wing. The nonlinearities tend to disappear with increase in Mach number, especially at supersonic

speeds. The addition of the horizontal tail creates an end-plate effect on the vertical tail which has a large stabilizing effect on the yawing moments. This large effect is due not only to the increase in lateral force on the vertical tail but also to a rearward shift of the center of the vertical tail load, as indicated in figure 8.

The variation of the directional stability derivative C_{n_β} with Mach number for the tail-off configuration and for the complete model is shown in figure 9 for sideslip angles between 0° to 5°. The derivatives were evaluated by taking the slope of the faired C_n curves at the desired values of β. The data for the tail-off configuration show that C_{n_β} decreases up to a Mach number of approximately 1.00. The tail-on configuration shows a large increase in stability, with increasing Mach number, most of which can be attributed to an increase in $dC_Y/d\beta$ of the vertical tail. An increase in moment arm, that is a rearward shift of center of load on the vertical tail with increasing Mach number, as indicated in figure 8, also contributes to the increased stability.

At subsonic Mach numbers, the addition of tip tanks had little effect on the yawing-moment coefficients of the model (fig. 10). An increase of stability noted at supersonic speeds was directly connected with an increase in lateral force.

Rolling moment due to sideslip.- The wing-body configuration shows a linear variation of rolling-moment coefficient with angle of sideslip at all test Mach numbers (fig. 7). Again, with the addition of the vertical tail, nonlinearities are present at low Mach numbers and vanish at supersonic speeds.

The addition of the horizontal tail, as previously mentioned, increases the side force on the vertical tail and also shifts the center of load upward. Furthermore, the horizontal tail contributes to the rolling moment because of the asymmetric load on the horizontal tail. The combined effects produced about a 75-percent increase in rolling-moment coefficient over that of the vertical tail alone. It was for this reason that large negative dihedral of the wings is required to oppose the strong rolling-moment effect of the horizontal tail.

The effect of Mach number on the effective dihedral derivative C_{l_β} is shown in figure 11 for both the wing-body configuration and the complete model. The positive rolling moment due to sideslip for the wing-body configuration increases slightly with Mach number because the lift-curve slope of the wing increases with Mach number. However, when the empennage is added, C_{l_β} becomes more negative with Mach number because of the greater increase in the lift-curve slope of the vertical tail $dC_Y/d\beta$ (as indicated in fig. 7).

The addition of wing tip tanks decreases the effective dihedral as much as 50 percent at the low Mach numbers (see fig. 11) although the variation with Mach number remained similar to the configuration without tanks.

Lateral Characteristics at Lifting Conditions

Yawing moments.- The basic data are presented in figure 12 and the derivatives are presented in figure 13. With an increasing lift coefficient, the yawing moments of the wing-fuselage configuration generally increased which resulted in C_{n_β} becoming more unstable. These results are contrary to reference 4 which predicts an increase of stability for wings of aspect ratio 6 or higher with negative dihedral. The discrepancy is possibly due to the fact that the effect of the induced drag, which is destabilizing, is larger than the stabilizing effect of the lift vector for low-aspect-ratio wings. At Mach numbers of 0.80 and 0.90 at the high values of lift coefficient, C_{n_β} becomes more stable. The reason for this trend could be that the center of load moves inboard on the trailing wing which reaches stall before the leading wing.

For the model with the vertical tail or with the vertical and horizontal tail, the static stability remained stable for all Mach numbers and C_L values. The yawing moments of the model with vertical tail tend to become more stable with increase in C_L up to lift coefficients of 0.4 or above depending on Mach number (fig. 13). Since the side force increases steadily with increasing C_L, the change in yawing moments at the higher values of lift is apparently due to a forward movement of center of load on the vertical tail. Comparison of C_{n_β} with and without the horizontal tail (fig. 13) shows that the magnitude of the values is greatly increased by the addition of the horizontal tail although the variation of C_{n_β} with C_L remains essentially the same as for the model with vertical tail alone.

Rolling moments.- The rolling moment of the wing-fuselage configuration at zero lift (fig. 13) gave positive values of C_{l_β} or negative effective dihedral. With increasing lift, C_{l_β} tends to become more negative. At the low Mach numbers, the change in the C_{l_β} curves at C_L of 0.7 was due to wing stall.

A decrease in effective dihedral with increasing C_L (fig. 13) is due to the fact that the coefficient C_l is referred to the stability axis system. In figure 12(b), the rolling-moment coefficients for the body axes system are plotted at $M = 1.06$ (dashed line) and show that

C_l is constant through the lift-coefficient range of this test. The same trend would be observed at the lower Mach numbers, and in fact at M = 0.80 and 0.90, C_l would become more stable at high C_L values. With the addition of the horizontal tail (fig. 12(c)), the magnitude of the C_l values is increased but the trends remain the same as for the model with vertical tail only. Figure 13 shows that positive effective dihedral existed for the complete model through the lift and Mach number range tested. The values of C_{l_β} increased with Mach number for the low-lift case and decreased at the high values of lift.

Shock patterns associated with sideslip.- A comparison of the plan-view shadowgraph pictures for sideslip angles of 0° and 5° is shown for several configurations in figure 14. Generally, the shock-wave position was little affected by yawing the model, but shock angles were skewed. The thickness of the boundary layer on the leeward side is indicated by the diffusing of the strong shock front near the fuselage ahead of the duct. (See fig. 14(b) and 14(c).) It appears that the boundary layer would be sufficiently thick to allow only relatively low energy air to enter this inlet and thus there exists the possibility of unstable internal flow and reduced thrust.

Lateral and Directional Controls

Effects of aileron on rolling and yawing moments.- The variations of C_l and C_n with C_L for 20°, -10°, and -20° left aileron deflection and for various Mach numbers are shown in figure 15 for the complete model. The rolling moment above Mach number 0.95 generally decreases with increasing C_L for positive deflections. For the lower Mach numbers the rolling moment increases up to where separation starts on the wing. Negative deflection generally produced constant roll with C_L for most of the test conditions. The rolling moments are similar with and without the horizontal tail; see figures 15(c) and 15(d).

Aileron effectiveness is indicated in figure 16 for a range of Mach number. Control effectiveness remained nearly linear at the low Mach numbers and zero-lift coefficients. However, at moderate and high lift coefficients, as indicated in the figure at $C_L = 0.8$, control effectiveness decreased for negative deflection and increased for positive deflections of the aileron for the low Mach numbers. At the higher Mach numbers, both negative and positive deflections produced linear variations of C_l for all lift coefficients. The total aileron effectiveness for a left and right aileron was constant for lift coefficients up to about 0.8 and for the Mach number range tested. Above this lift coefficient the aileron effectiveness decreased particularly at the low Mach numbers.

The yawing moments are negative for negative deflections (left aileron up) (figs. 15(a) and (b)) at zero lift coefficient, and becomes less negative with increasing lift. For positive deflection of the left aileron (figs. 15(c) and (d)), yawing moments are positive at zero lift coefficient and become negative with increasing lift. These characteristics are peculiar in that generally the increased drag on a left wing due to aileron deflection (positive or negative) causes a negative yawing moment. Since this wing has appreciable negative dihedral, the side component of the additional force normal to the wing surface caused by deflecting the aileron will be outward for a positive deflection of the control surface and vice versa for negative deflection. In both cases, favorable yaw will result since the center of gravity is sufficiently forward of the ailerons to yield favorable yawing conditions. The magnitude of the side force involved is shown in figure 15(e) for $\pm 20^\circ$ aileron deflection.

Assuming 1 to 1 differential ailerons, favorable yawing moments will be produced for most Mach numbers through a C_L of at least 1.00. The total yawing-moment coefficient due to aileron deflection will decrease with increasing lift coefficient.

Rudder and yaw damper effectiveness.- Lateral characteristics through the sideslip range with the rudder deflected are shown in figure 17(a). In general, the results indicate that the slopes of the curves changed slightly with rudder deflection. Similar tendencies are shown for the yaw damper deflected -20° in figure 17(b). Rudder and yaw damper effectiveness $C_{n_{\delta_r}}$ and $C_{n_{\delta_d}}$ with Mach number is best shown in figure 18 for three sideslip angles. Although the rudder effectiveness parameter $C_{n_{\delta_r}}$ remained fairly constant through the tested Mach number range, the required rudder effectiveness increased with Mach number for constant control response due to the increase of C_{n_β} with Mach number. For example, a study of figures 9 and 18 shows that 2° of rudder deflection produced about 1° of sideslip for small angles of sideslip and low Mach numbers, while at a Mach number of 1.00, 2° of rudder deflection produced about $\frac{1^\circ}{2}$ of sideslip. For sideslip angles of $\pm 5^\circ$, the effectiveness of the rudder increases and decreases, respectively, from the effectiveness at 0° of sideslip.

The yaw damper effectiveness parameter $C_{n_{\delta_d}}$ which was -0.0005 at 0.80 Mach number decreased about 50 percent at a Mach number of 0.95.

CONCLUSIONS

The results of this investigation of the lateral stability and control effectiveness of a fighter-type airplane with a thin low-aspect-ratio wing and a tee-tail at Mach numbers of 0.80 to 1.06 indicated the following conclusions:

1. The static stability derivative C_{n_β} was positive for the lift coefficient and Mach number range tested, and increased up to a Mach number of 1.03.

2. Positive effective dihedral was indicated for the complete model through the Mach number and C_L range tested. The values of C_{l_β} increased with Mach number for the low-lift case, and decreased at the high values of lift.

3. The yawing moment due to aileron deflection was favorable for all Mach numbers tested through most of the C_L range. The total aileron effectiveness for a left and right aileron was fairly constant for lift coefficients up to about 0.8 and for the Mach number range tested. Above lift coefficient of 0.8 the aileron effectiveness decreased particularly at the low Mach numbers.

4. Yawing-moment effectiveness of the rudder changed little through the Mach number range. However, the sideslip due to rudder deflection decreased about 50 percent as a result of the increase of C_{n_β} with increasing Mach numbers from 0.80 to 1.06.

5. The yaw damper effectiveness parameter $C_{n_{\delta_d}}$ decreased by about 50 percent with an increase in Mach number from 0.80 to 0.95.

Langley Aeronautical Laboratory,
National Advisory Committee for Aeronautics,
Langley Field, Va., May 18, 1955.

REFERENCES

1. Sleeman, William C., Jr., and Wiggins, James W.: Experimental Investigation at High Subsonic Speeds of the Rolling Stability Derivatives of a Complete Model With an Aspect-Ratio-2.53 Wing Having an Unswept 72-Percent-Chord Line and a High Horizontal Tail. NACA RM L54I20, 1955.

2. Smith, Willard G.: Wind-Tunnel Investigation at Subsonic and Supersonic Speeds of a Fighter Model Employing a Low-Aspect-Ratio Unswept Wing and a Horizontal Tail Mounted Well Above the Wing Plane - Longitudinal Stability and Control. NACA RM A54D05, 1954.

3. Ward, Vernon G., Whitcomb, Charles F., and Pearson, Merwin D.: Air-Flow and Power Characteristics of the Langley 16-Foot Transonic Tunnel With Slotted Test Section. NACA RM L52E01, 1952.

4. Pearson, Henry A., and Jones, Robert T.: Theoretical Stability and Control Characteristics of Wings With Various Amounts of Taper and Twist. NACA Rep. 635, 1938.

TABLE I

DIMENSIONS OF THE MODEL

Wing Geometry:	
Root and tip airfoil section	Modified biconvex 3.4 percent thick (forward 50 percent elliptical, aft 50 percent circular arc)
Area, sq ft	1.406
Span, in.	22.50
Mean aerodynamic chord, in.	9.59
Root chord, in.	13.00
Tip chord, in.	5.00
Aspect ratio	2.5
Taper ratio	0.385
Sweep at 25 percent chord, deg	18.5
Incidence, deg	0
Dihedral, deg	-10
Leading-edge droop (about 14.75-percent local wing chord), deg	3
Ailerons:	
Area (each), sq ft	0.0351
Mean aerodynamic chord, in.	2.36
Horizontal Tail:	
Airfoil sections	Modified biconvex
Area, sq ft	0.356
Mean aerodynamic chord, in.	4.54
Aspect ratio	2.97
Tail length, 0.25 wing M.A.C. to 0.25 horizontal tail M.A.C., in.	17.27
Vertical Tail:	
Airfoil section	Modified biconvex
Area, sq ft	0.255
Span, in. measured from fuselage intersection to tip	5.49
Mean aerodynamic chord, in.	7.11
Aspect ratio	0.82
Tail length, 0.25 wing M.A.C. to 0.25 vertical tail M.A.C., in.	13.52
Yaw Damper:	
Area, sq ft	0.0078
Mean aerodynamic chord, in.	1.22
Rudder:	
Area, sq ft	0.02947
Mean aerodynamic chord, in.	1.49
Fuselage:	
Length, in.	47.619
Maximum frontal area, sq ft	0.1583
Fineness ratio	9.98
External fuel tanks:	
Fineness ratio	12.1
Maximum diameter, in.	1.716
Maximum frontal area, each, sq ft	0.001605

TABLE II

CONFIGURATIONS AND TEST RANGE

Configuration (a)	α, deg	β, deg
W	0	-5, -3, -1.5, 0, 1.5, 3, 5
WE	0	-5, -3, -1.5, 0, 1.5, 3, 5
WE_2	0	-5, -3, -1.5, 0, 1.5, 3, 5
WE_2	-2 to 16	0, -5
WVE_2	-2 to 16	0, -5
$WVHE_2$	-2 to 16	0, -5
WVE_2	0	-5, -3, -1.5, 0, 1, 1.5, 3, 5
$WVHE_2$	0	-5, -3, -1.5, 0, 1, 1.5, 3, 5
$WVHTE_2$	0	-5, -3, -1.5, 0, 1, 1.5, 3, 5
WVHE	0	-5, -3, -1.5, 0, 1, 1.5, 3, 5
WVH	0	-5, -3, -1.5, 0, 1, 1.5, 3, 5
$WVHE_2{}^r{}_{-10}$	0	-5, -3, -1.5, 0, 1, 1.5, 3, 5
$WVHE_2{}^d{}_{-20}$	0	-5, -3, -1.5, 0, 1, 1.5, 3, 5
$WVHE_2{}^a{}_{-20}$	-2° to 16°	
$WVHE_2{}^a{}_{-10}$	-2° to 16°	
$WVHE_2{}^a{}_{+20}$	-2° to 16°	
$WVE_2{}^a{}_{+20}$	-2° to 16°	

[a]Configurations are designated by use of the following symbols:

W	wing with droop leading edge plus fuselage
V	vertical tail
H	horizontal tail
T	tip tanks
E	modified afterbody with inlets faired (on)
E_2	modified afterbody with maximum mass flow (on, unfaired inlets)
r	rudder (subscript indicates deflections in deg)
d	yaw damper (subscript indicates deflections in deg)
a	ailerons (subscript indicates deflections in deg)

	Wing	Horizontal tail
Aspect ratio	2.5	2.97
Taper ratio	.385	.311
Area	202.5 in.^{2}	51.25 in.^{2}
Span	22.50	12.328
Root chord	13.00	6.341
Tip chord	5.00	1.974
Section	Modified biconvex	Modified biconvex
Thickness ratio		
Root	3.4 percent	5 percent
Tip	3.4 percent	3 percent

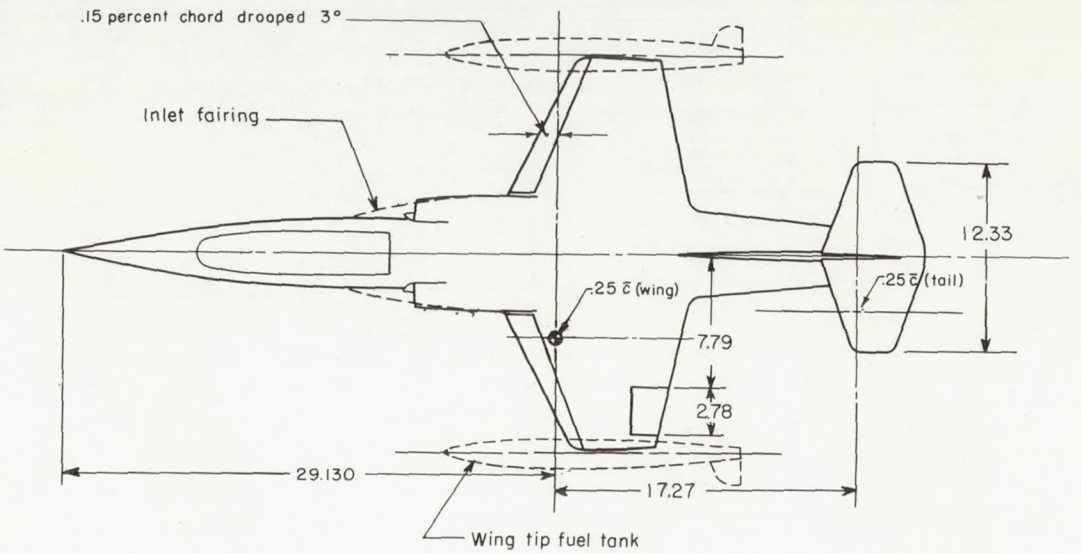

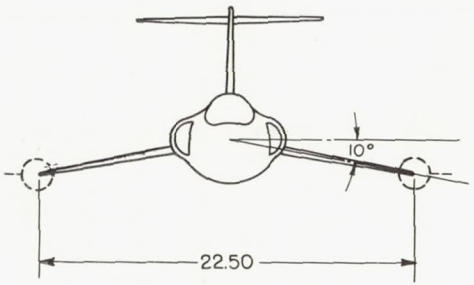

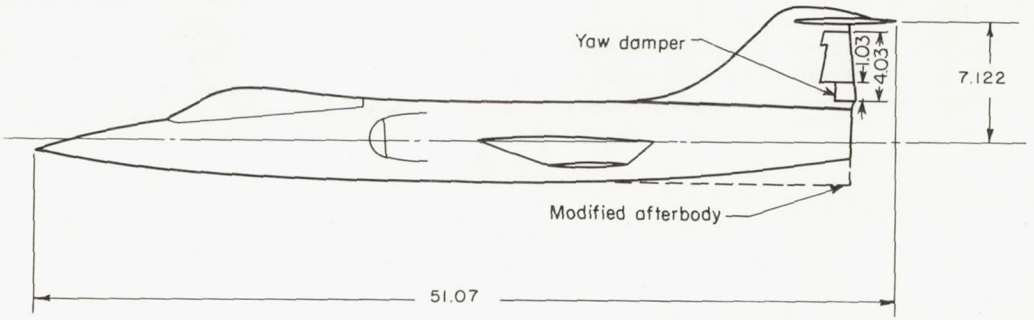

Figure 1.- General arrangement of the model. All dimensions in inches.

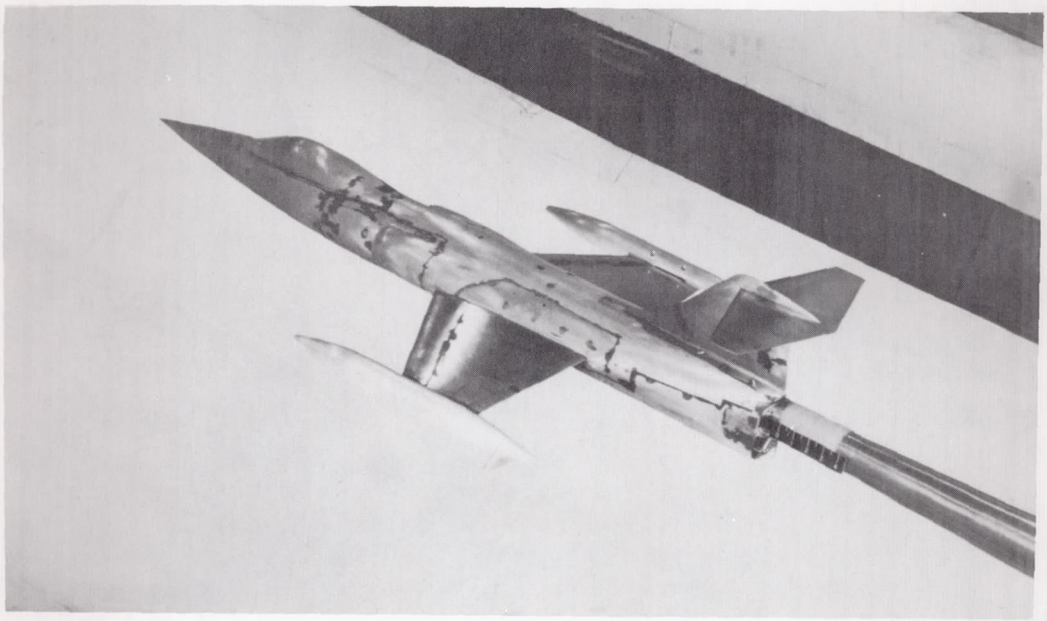

Complete configuration with tip tanks and internal flow ducting.

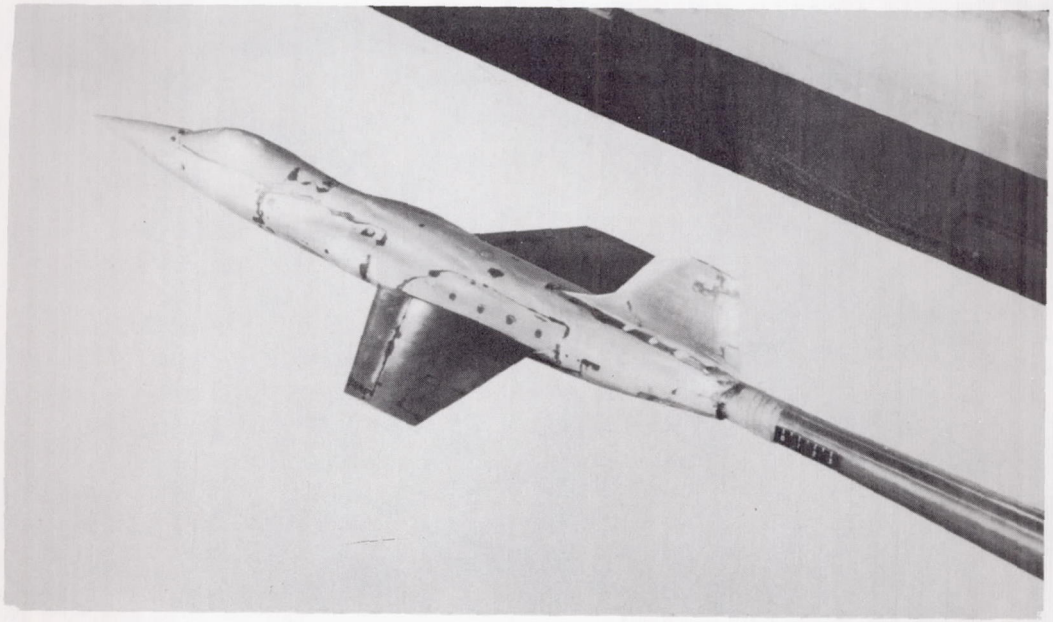

Faired inlet configuration without horizontal tail.

L-89358

Figure 2.- Typical configurations of the model.

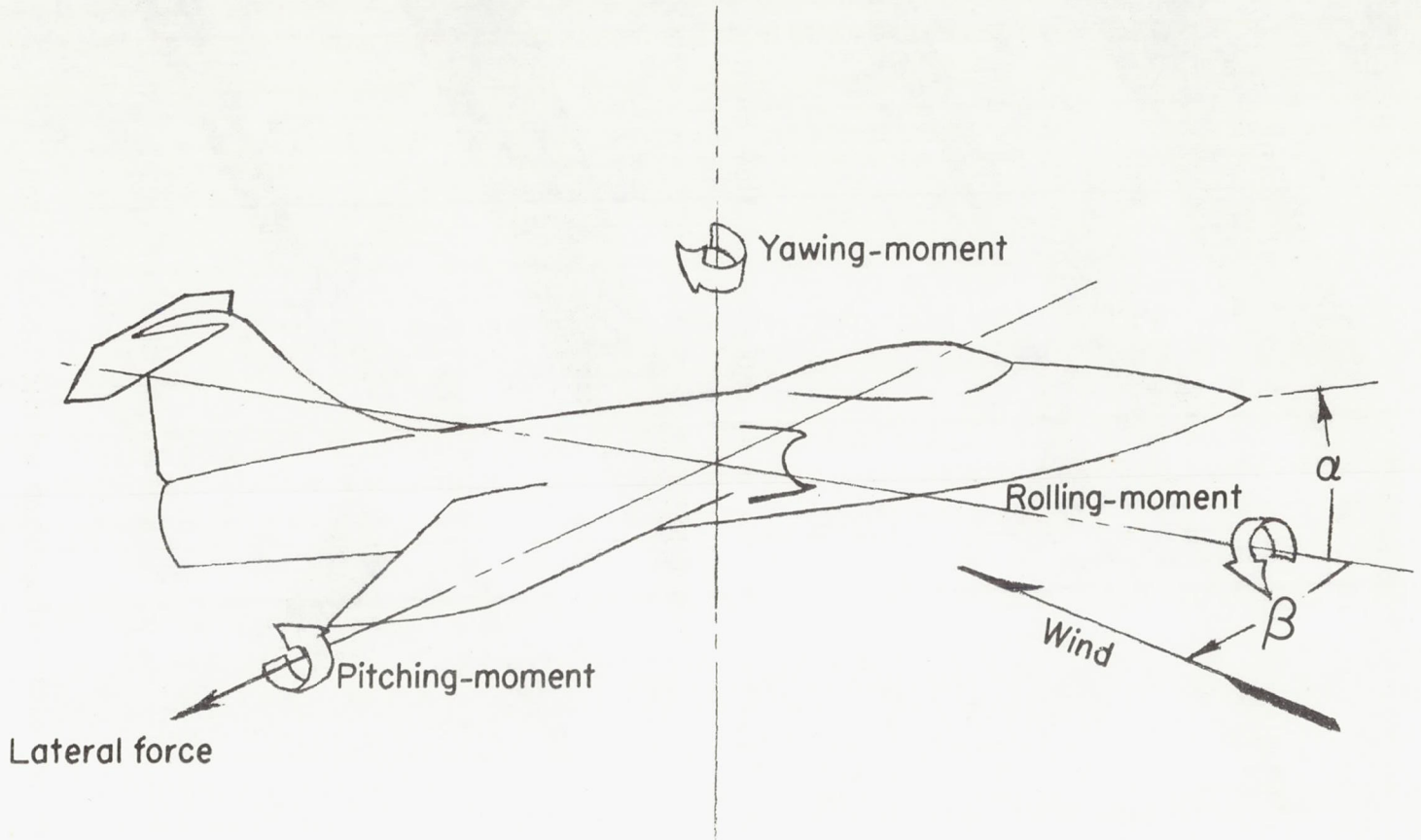

Figure 3.- Stability system of axis showing direction of positive values.

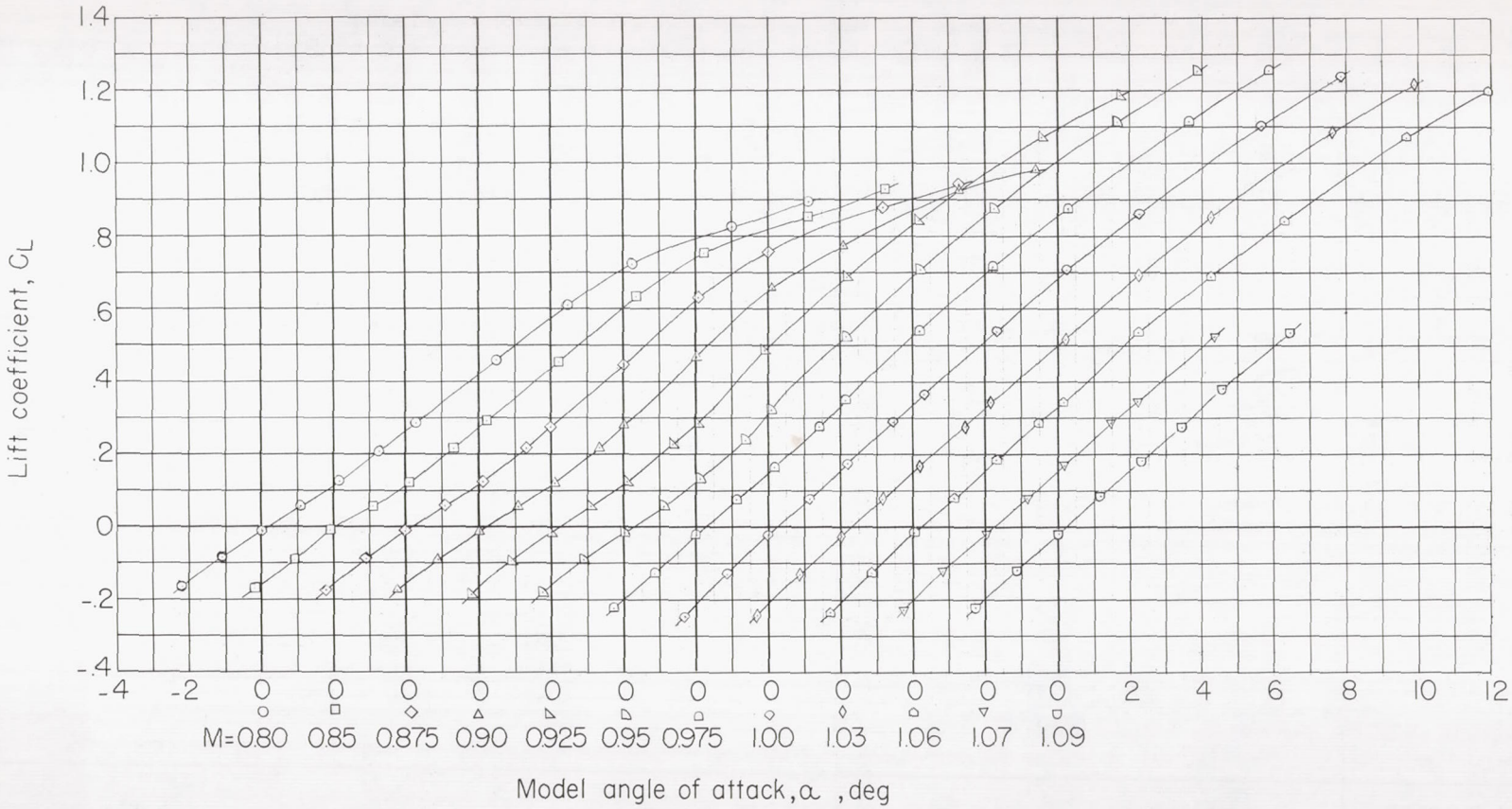

Figure 4.- Lift characteristics for the complete configuration, $WVHE_2$.

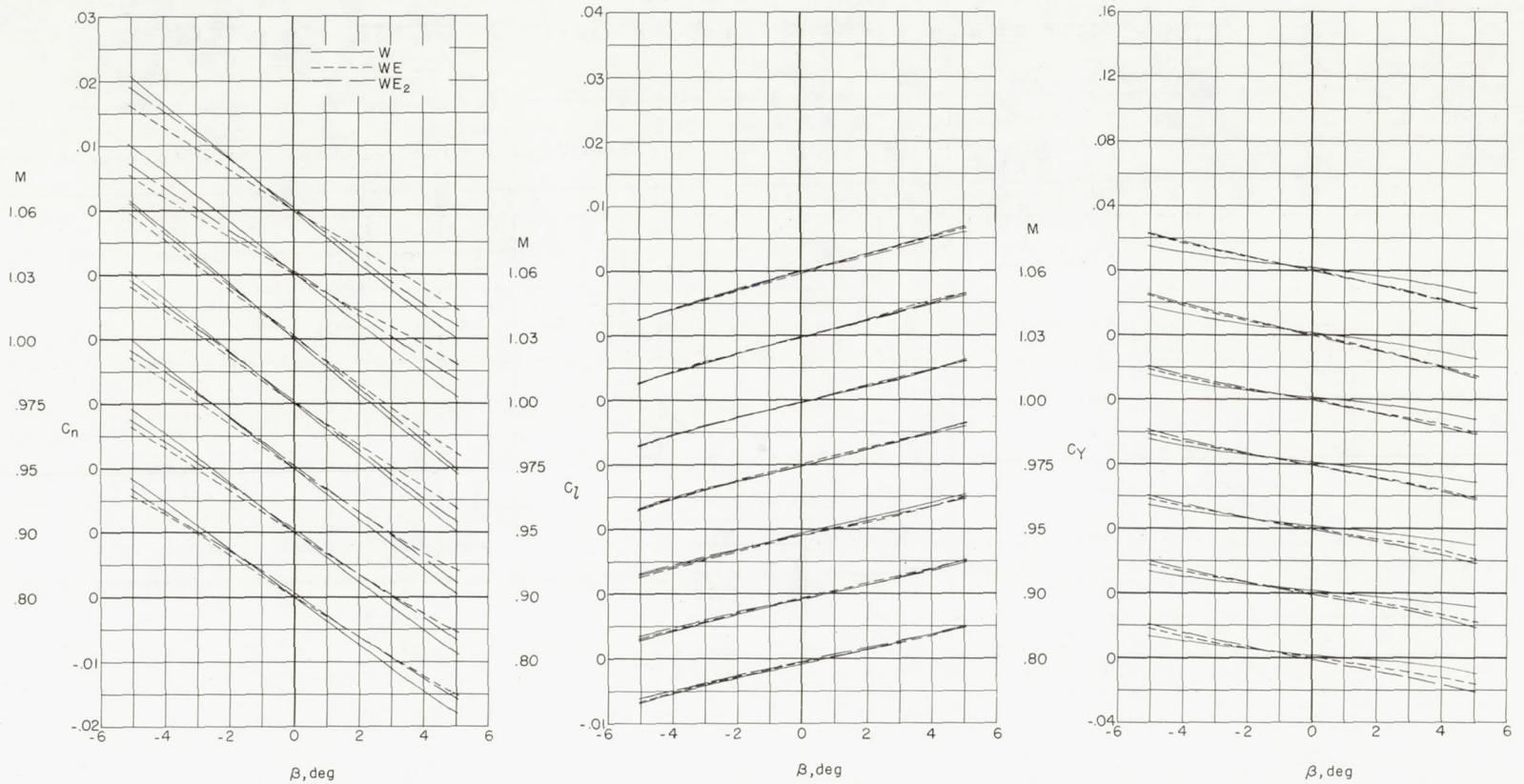

Figure 5.- Effect of the modified afterbody and internal flow on the lateral characteristics of the model without tail. $\alpha = 0^{\circ}$.

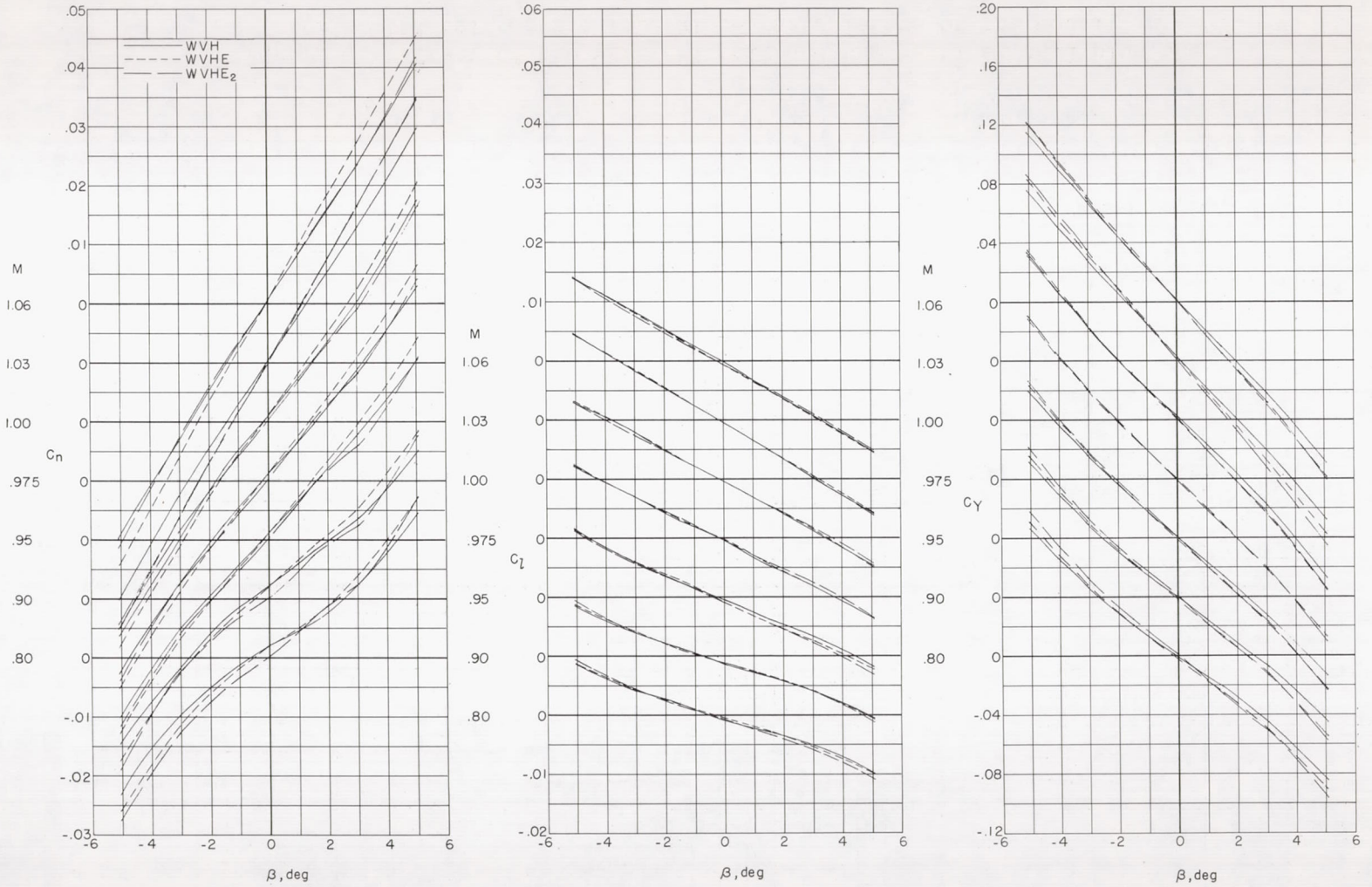

Figure 6.- Effect of the modified afterbody and internal flow on the lateral characteristics of the complete model. $\alpha = 0^{\circ}$.

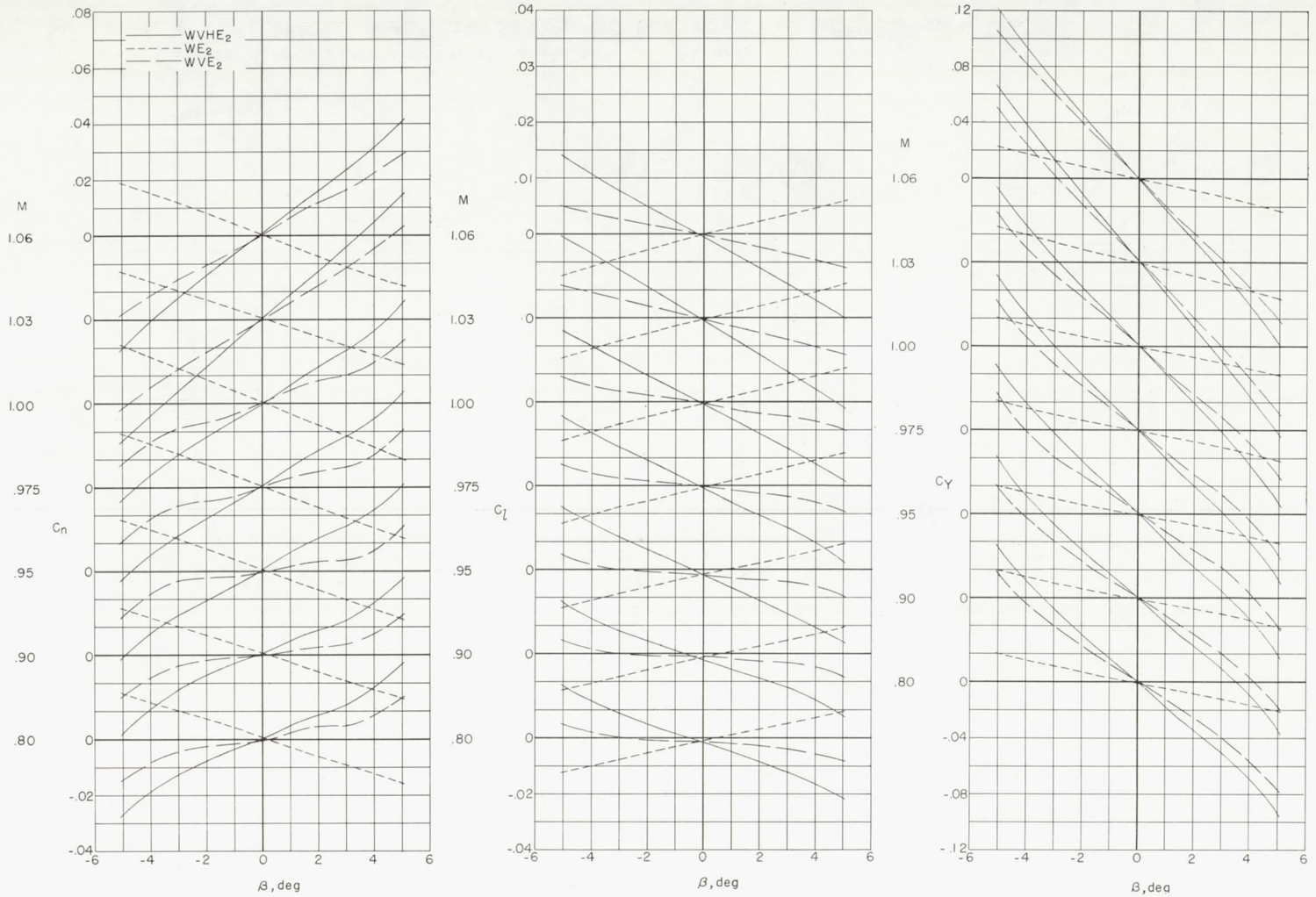

Figure 7.- Effect of the vertical tail and the vertical tail plus the horizontal tail on the lateral characteristics of the model. $\alpha = 0^{\circ}$.

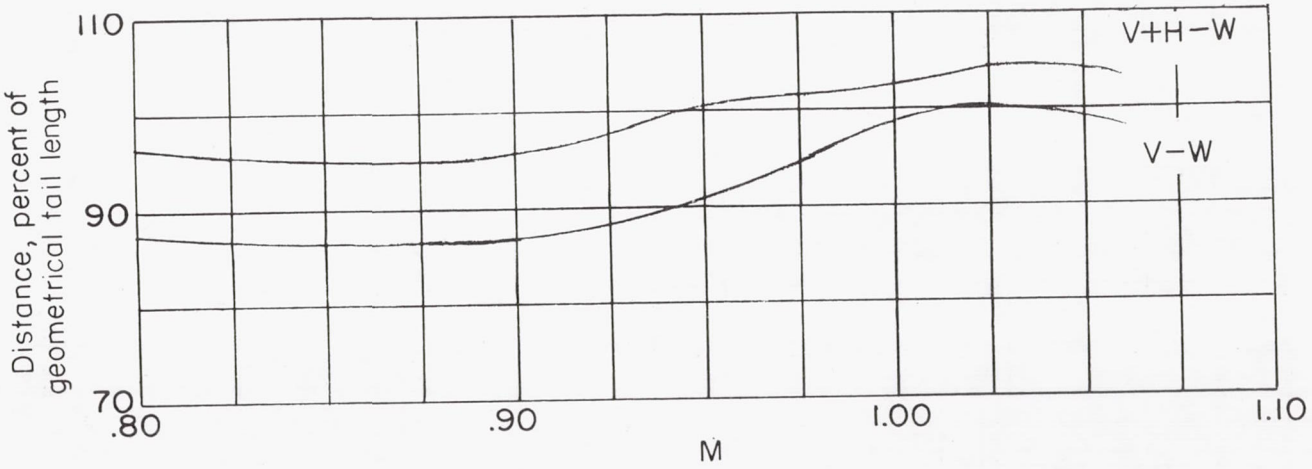

Figure 8.- Variation with Mach number of the longitudinal center-of-load location on the vertical tail including the effect of the horizontal tail.

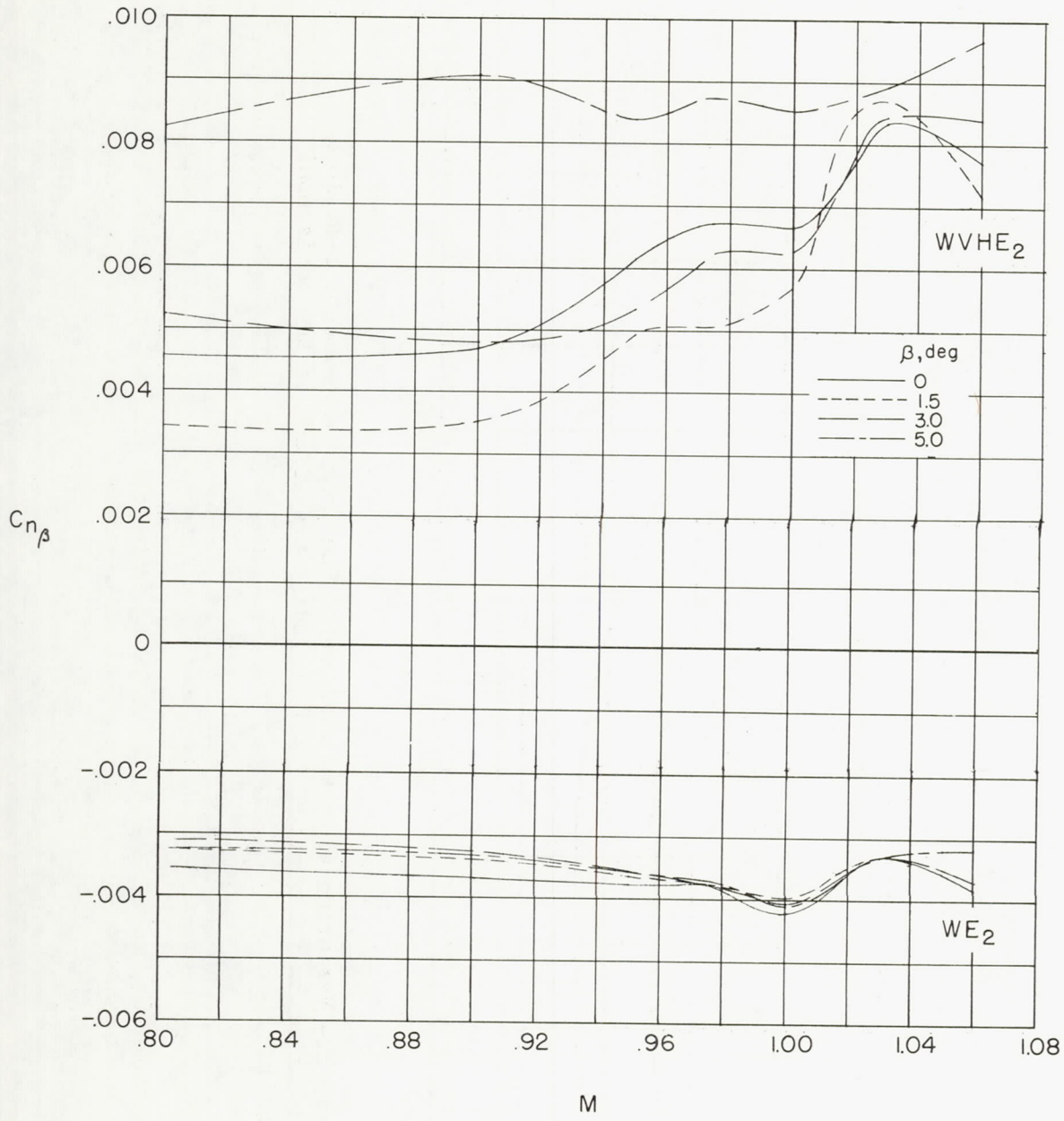

Figure 9.- Variation with Mach number of the yawing moment due to sideslip, $\alpha = 0^{\circ}$.

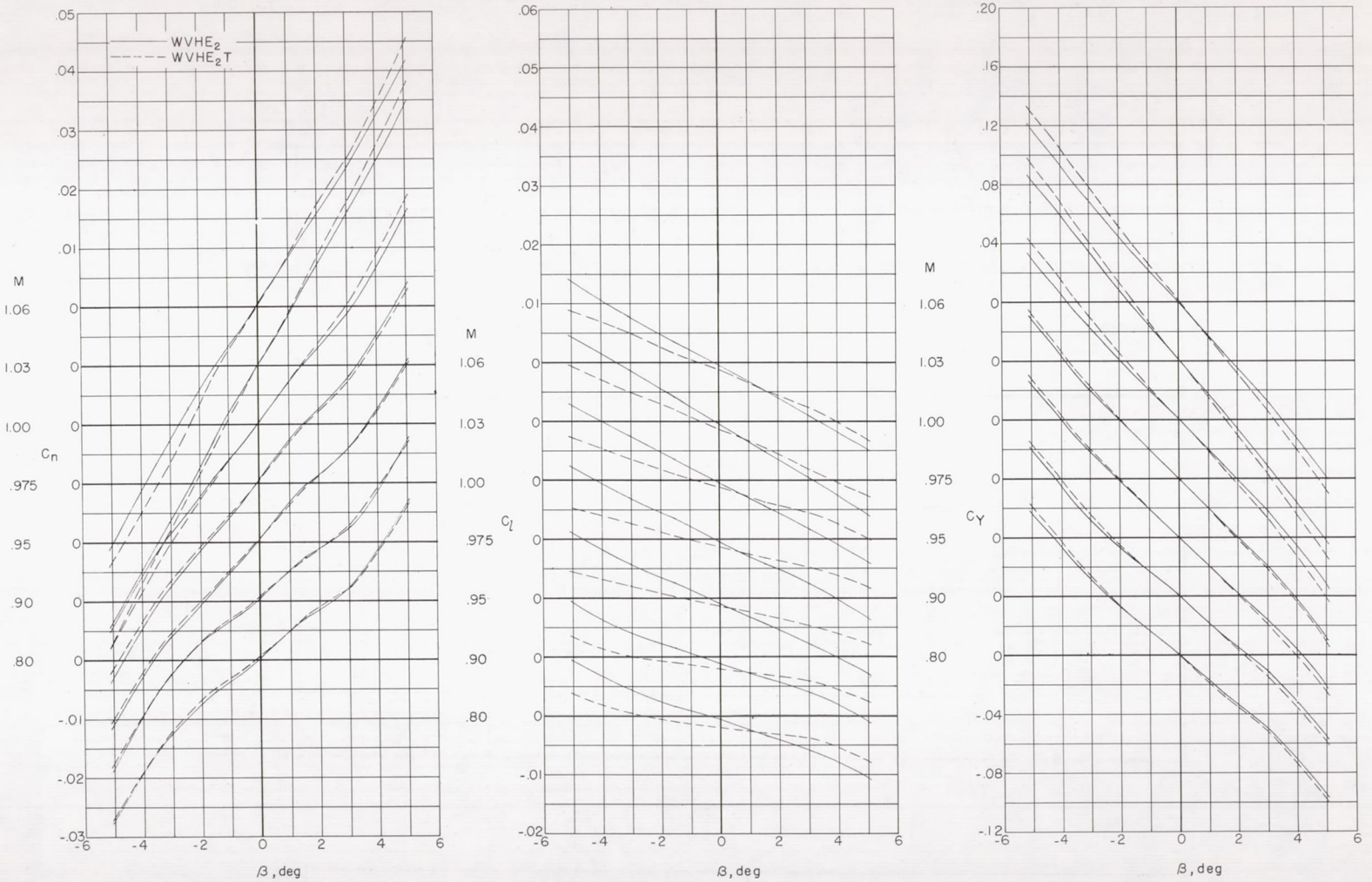

Figure 10.- The effect of tip tanks on the lateral characteristics of the model. $\alpha = 0^{\circ}$.

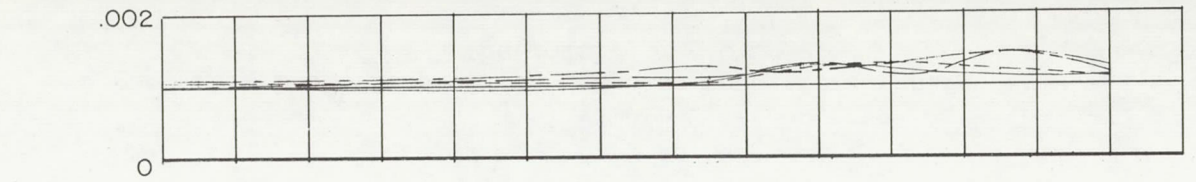

(a) WE_2.

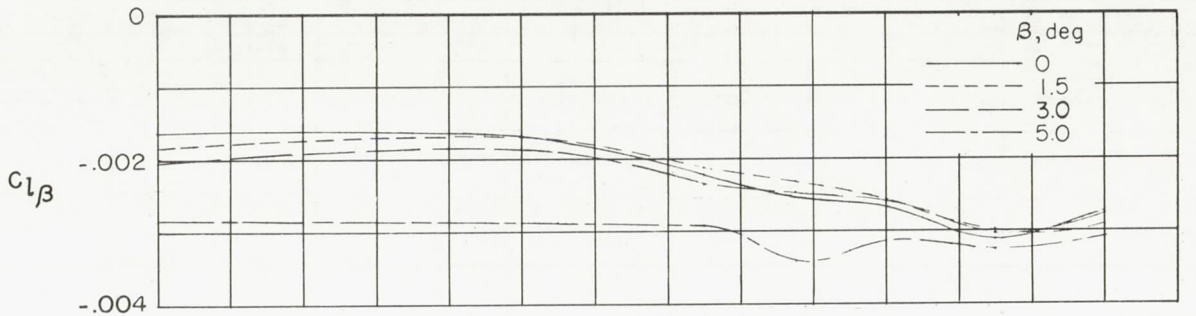

(b) $WVHE_2$.

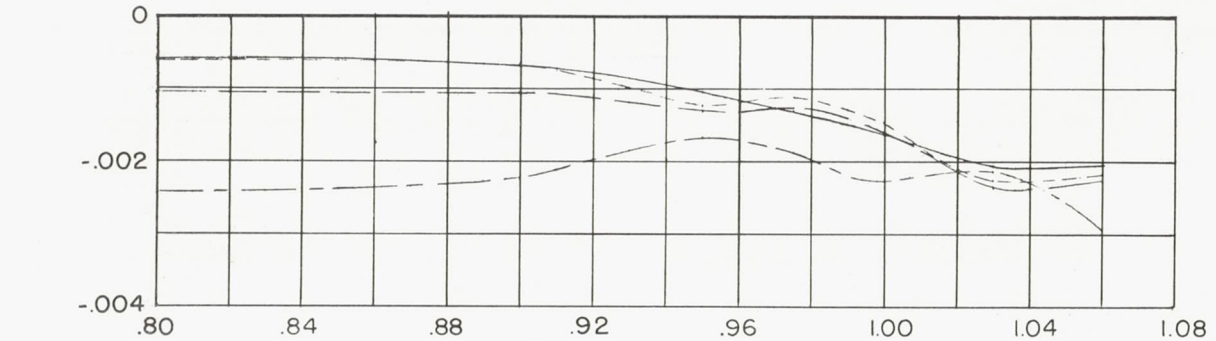

(c) $WVHE_2T$.

Figure 11.- Variation with Mach number of the rolling moment due to sideslip for several configurations. $\alpha = 0^\circ$.

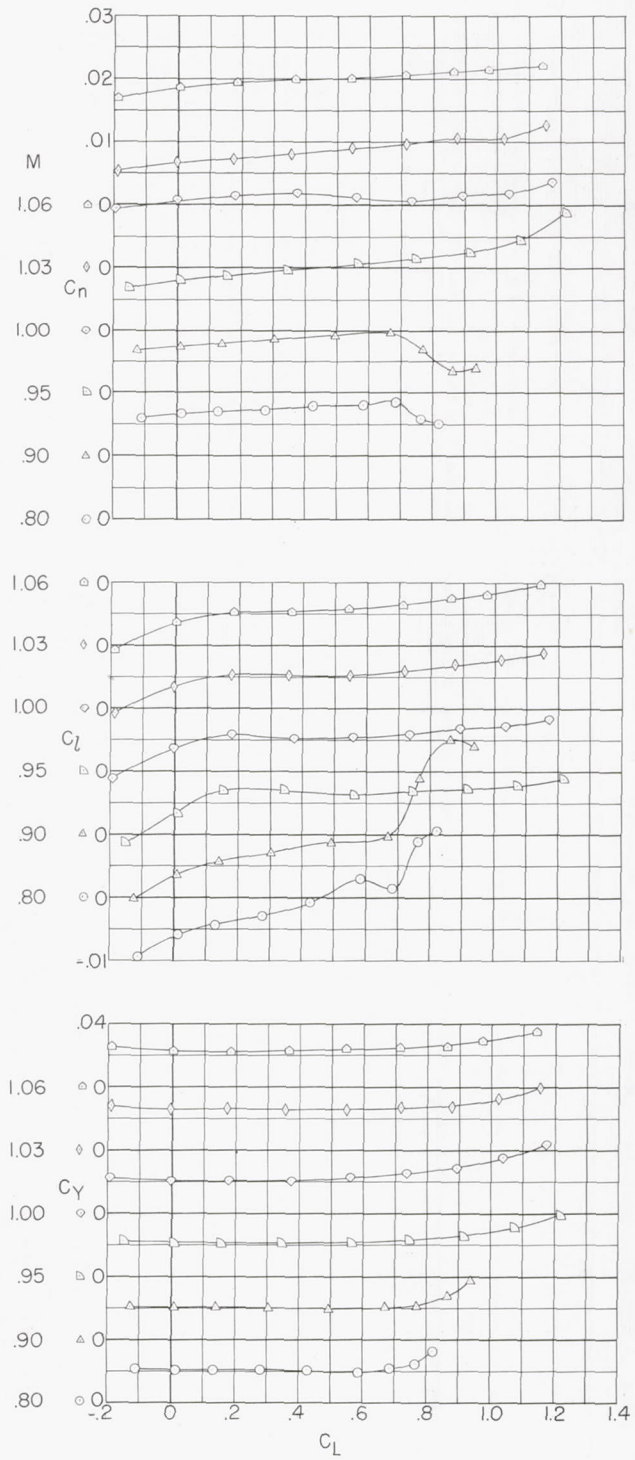

(a) WE_2.

Figure 12.- Lateral characteristics of lifting conditions for $\beta = -5^{\circ}$.

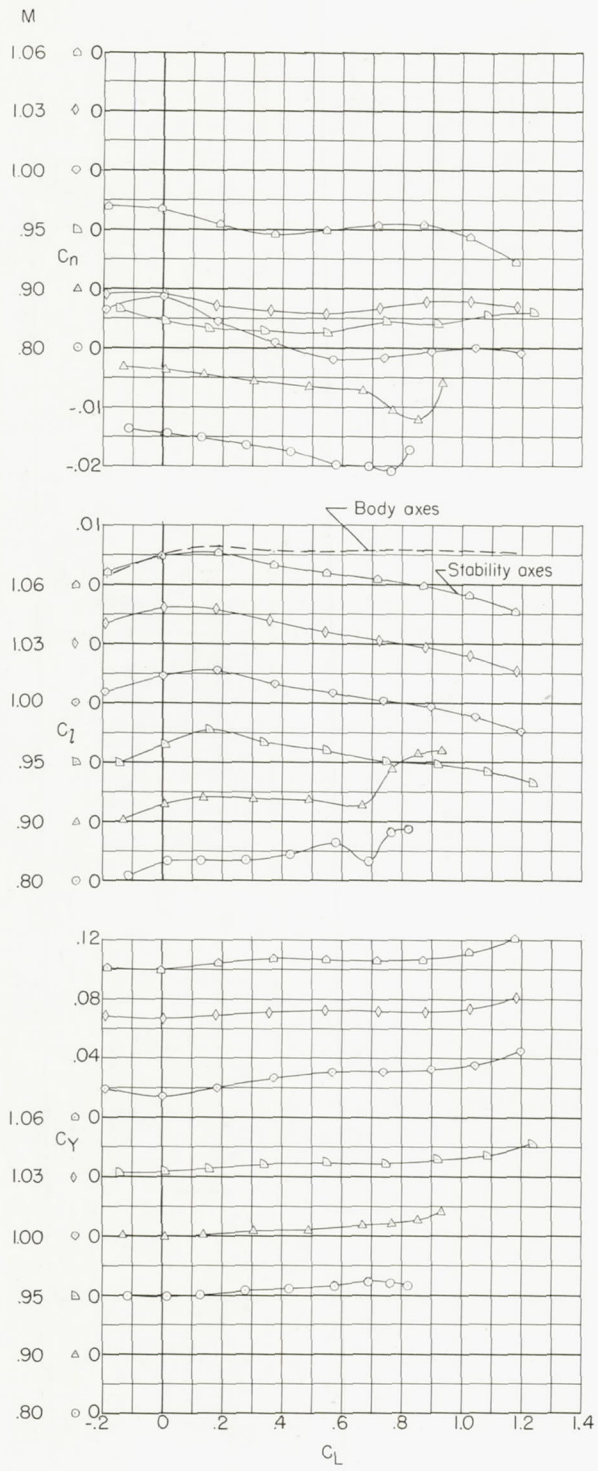

(b) WVE_2.

Figure 12.- Continued.

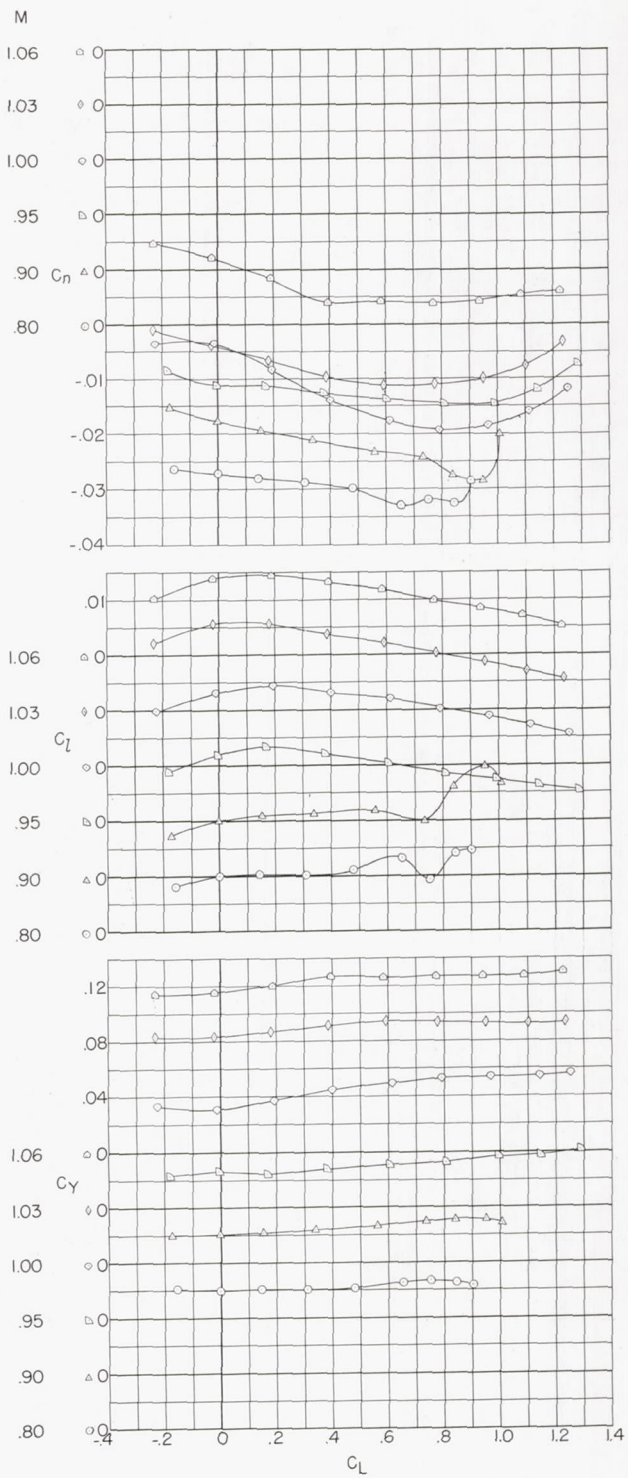

(c) $WVHE_2$.

Figure 12.- Concluded.

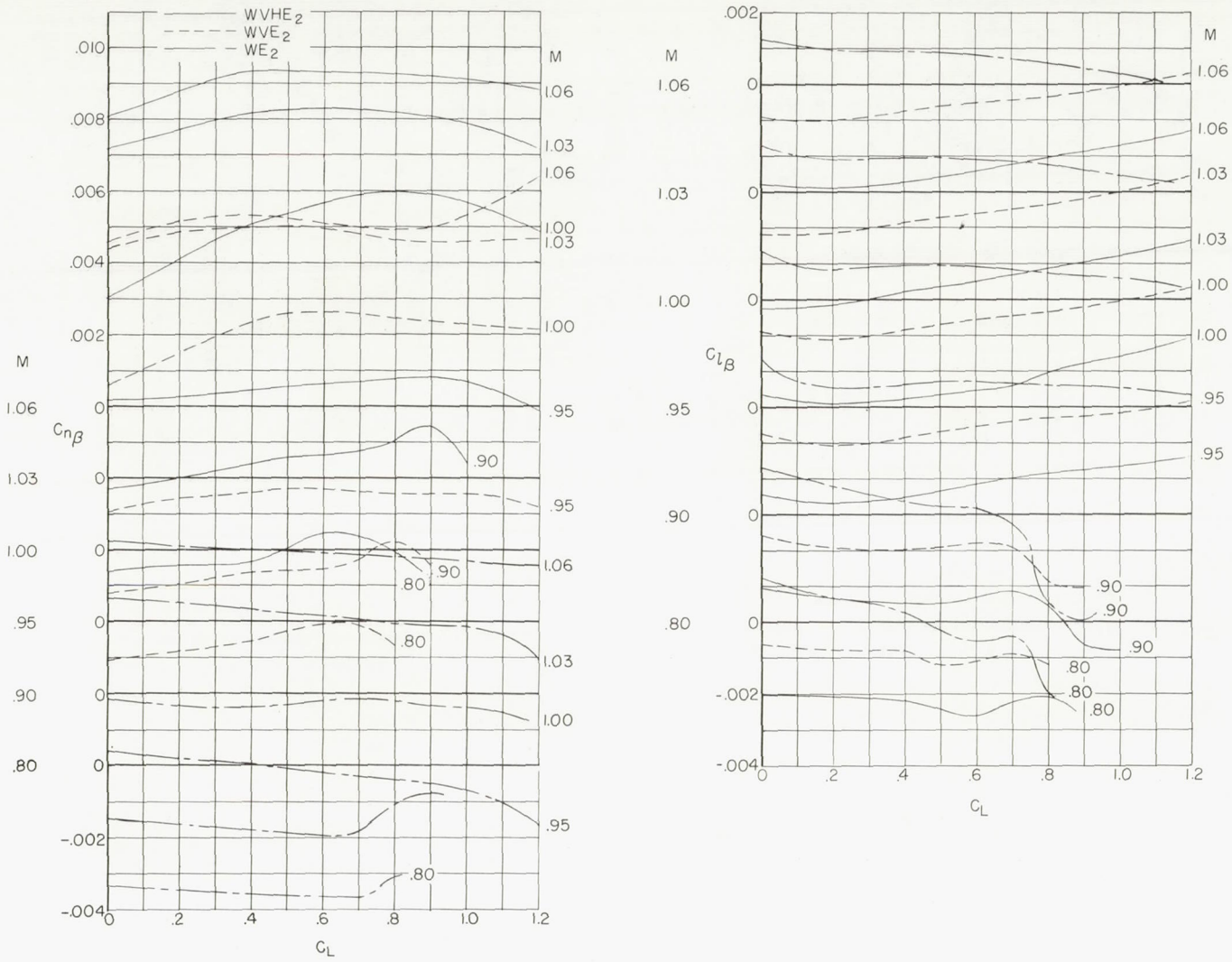

Figure 13.- Effect of lift on the static derivatives. $\beta = -5^{\circ}$.

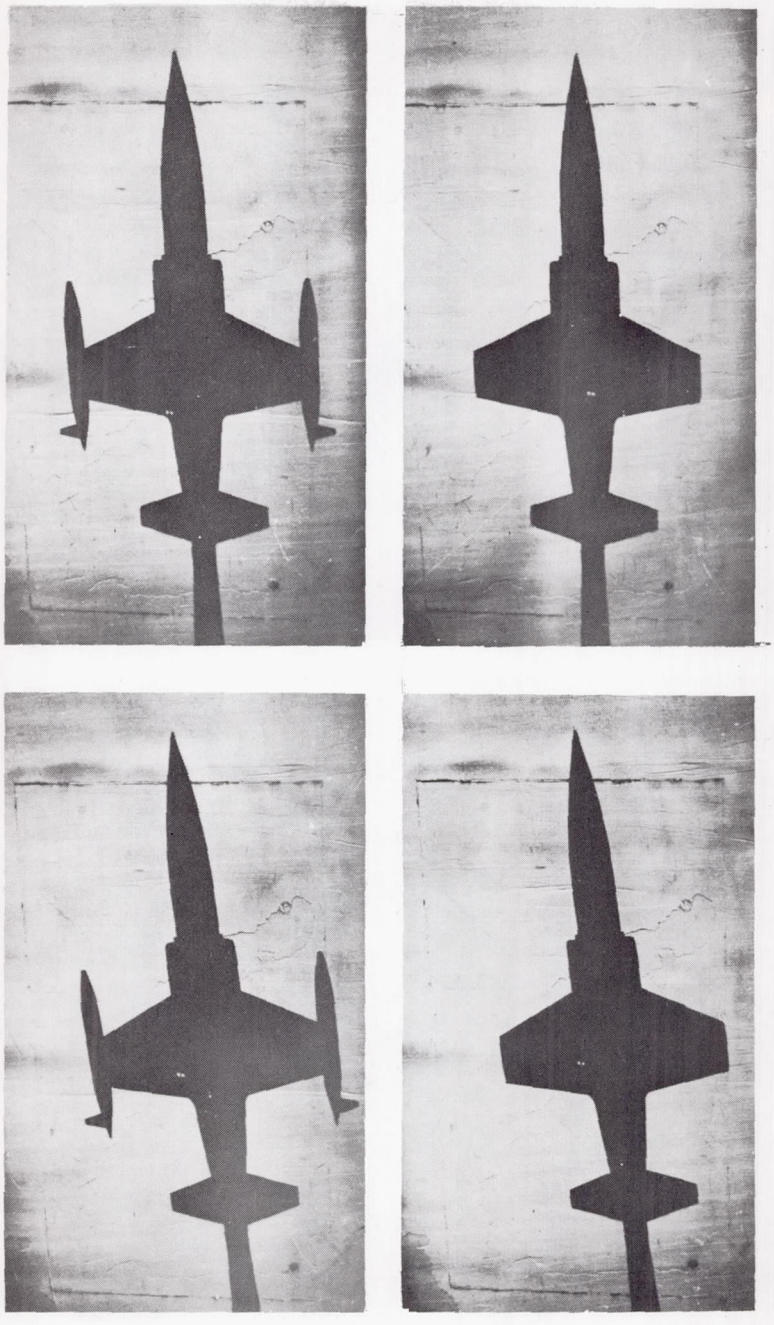

L-89359

(a) M = 0.95.

Figure 14.- Plan-view shadowgraphs of several model configurations. β is 0° for the upper photographs and 5° for the lower photographs.

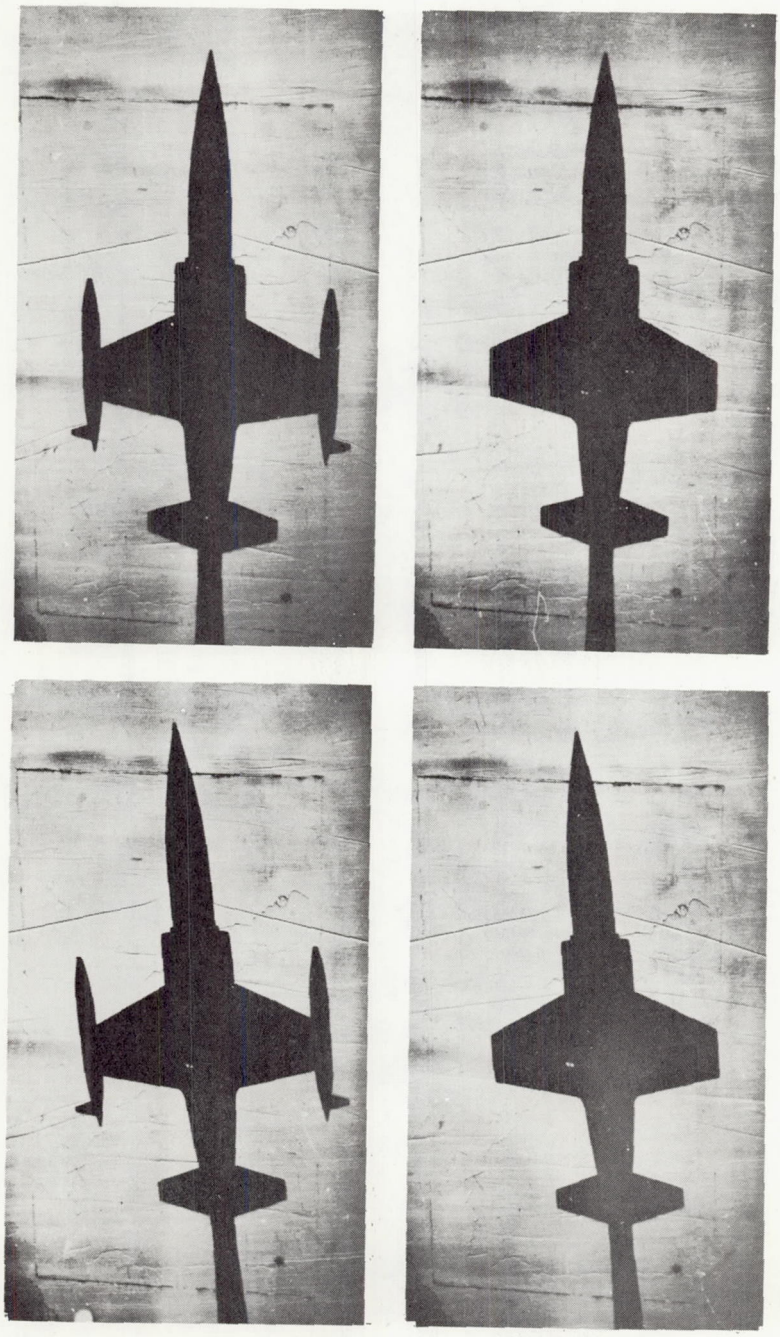

WVHE$_2$T WVHE$_2$

L-89360

(b) M = 1.00.

Figure 14.- Continued.

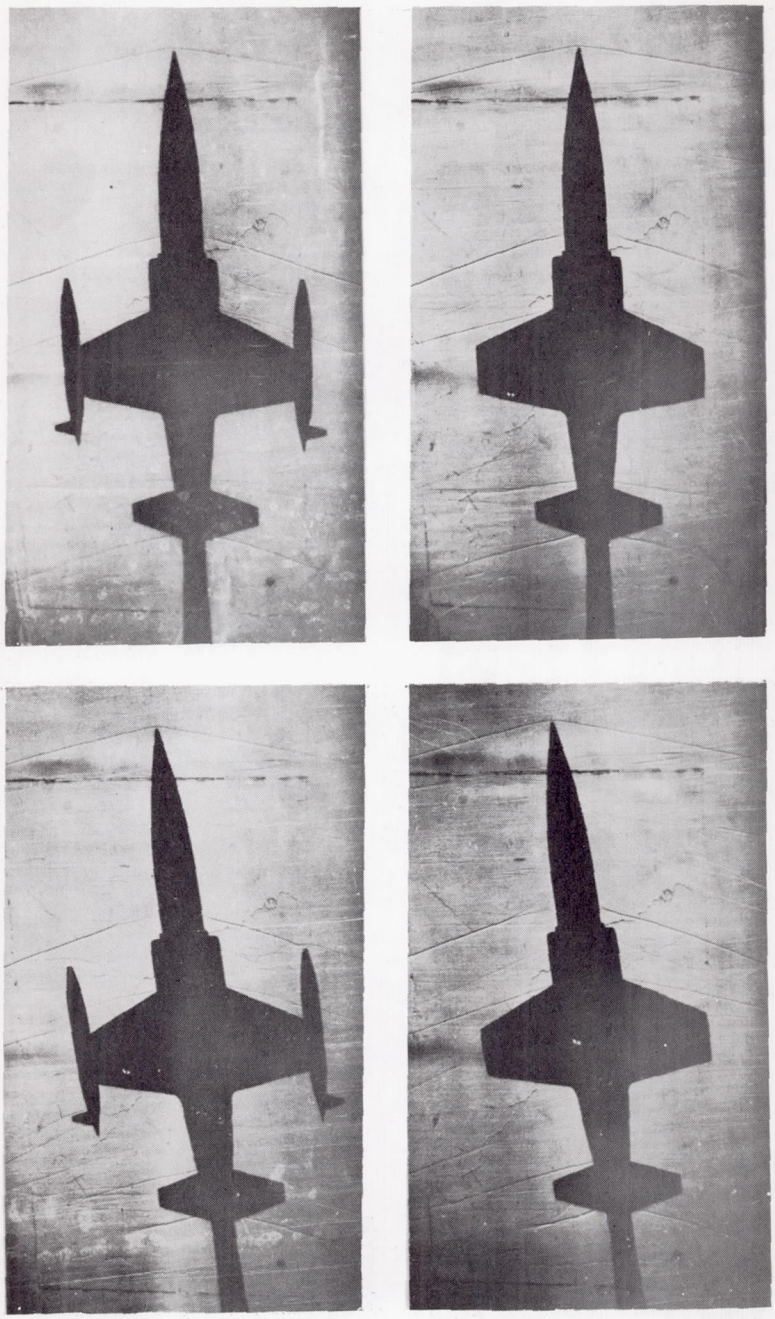

WVHE$_2$T WVHE$_2$

L-89361

(c) M = 1.06.

Figure 14.- Continued.

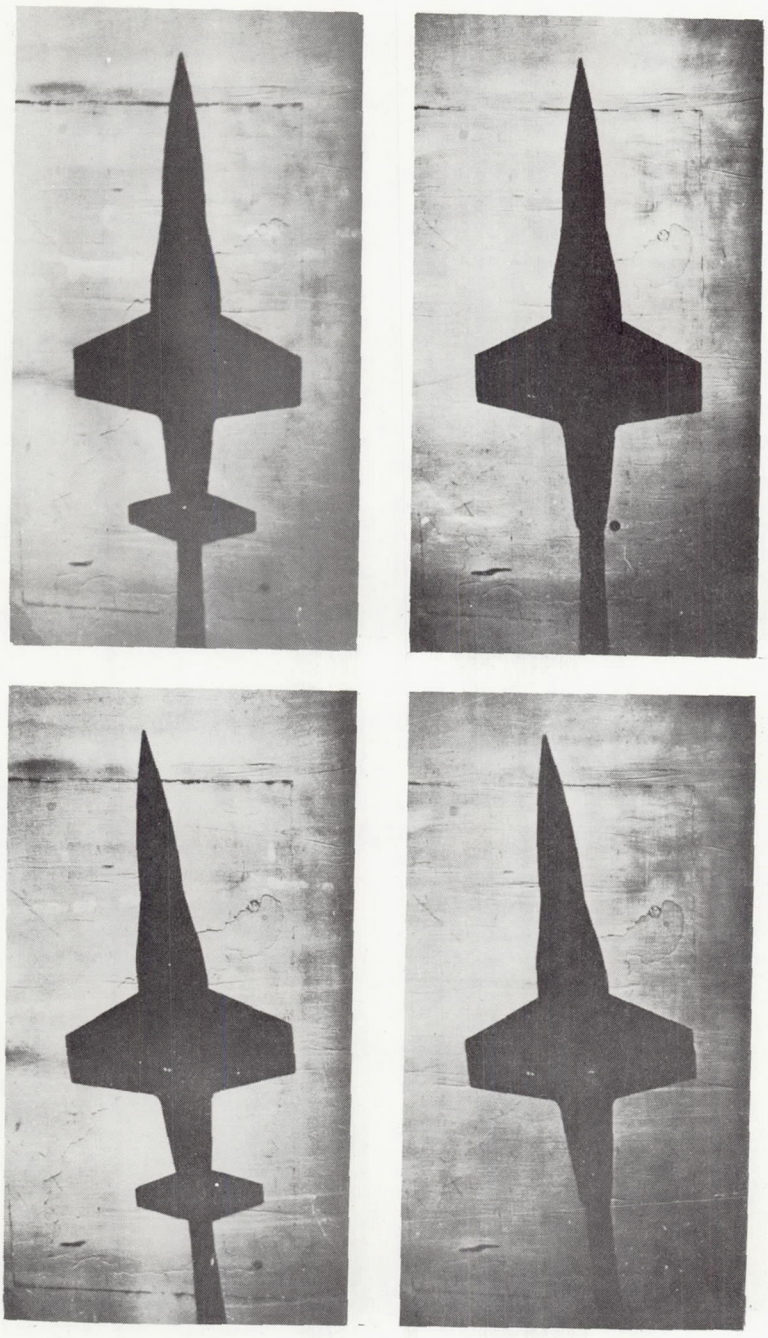

(d) M = 0.95.

Figure 14.- Continued.

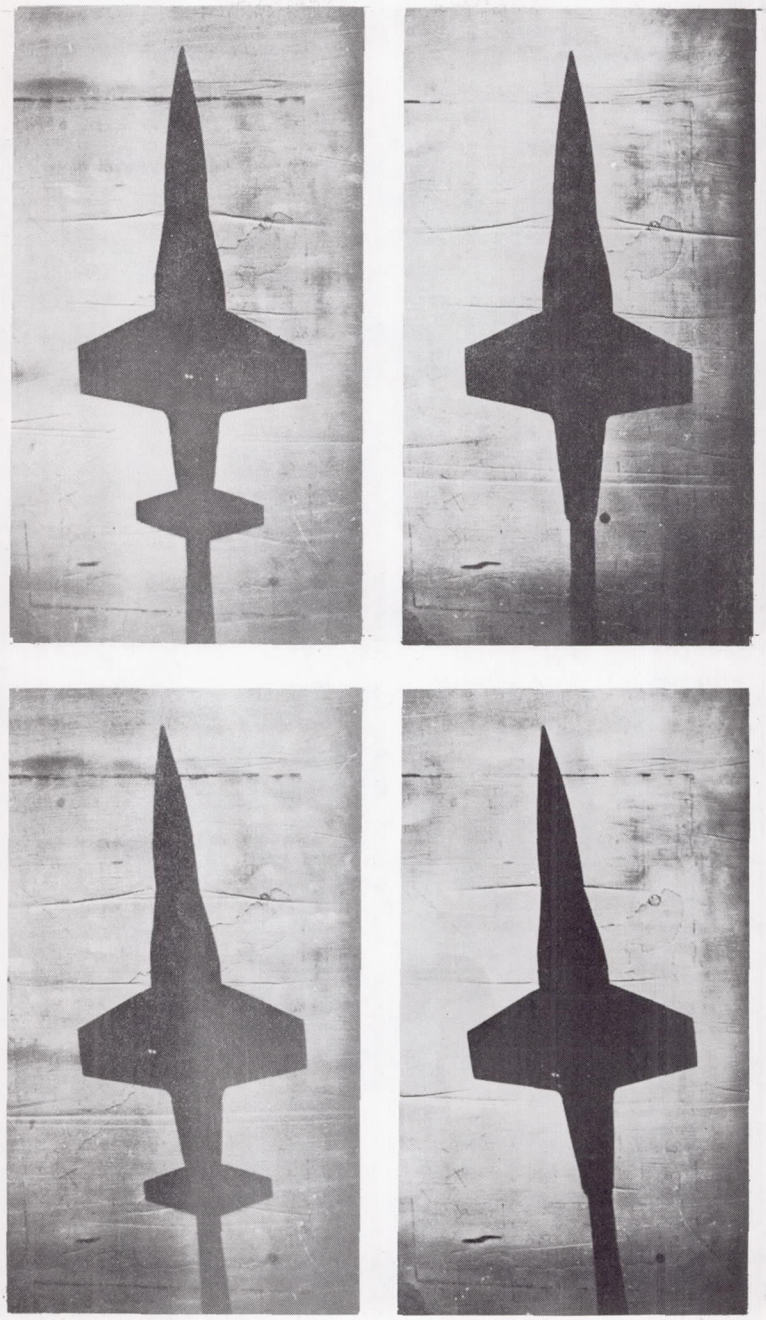

WVH W

L-89363

(e) M = 0.975.

Figure 14.- Continued.

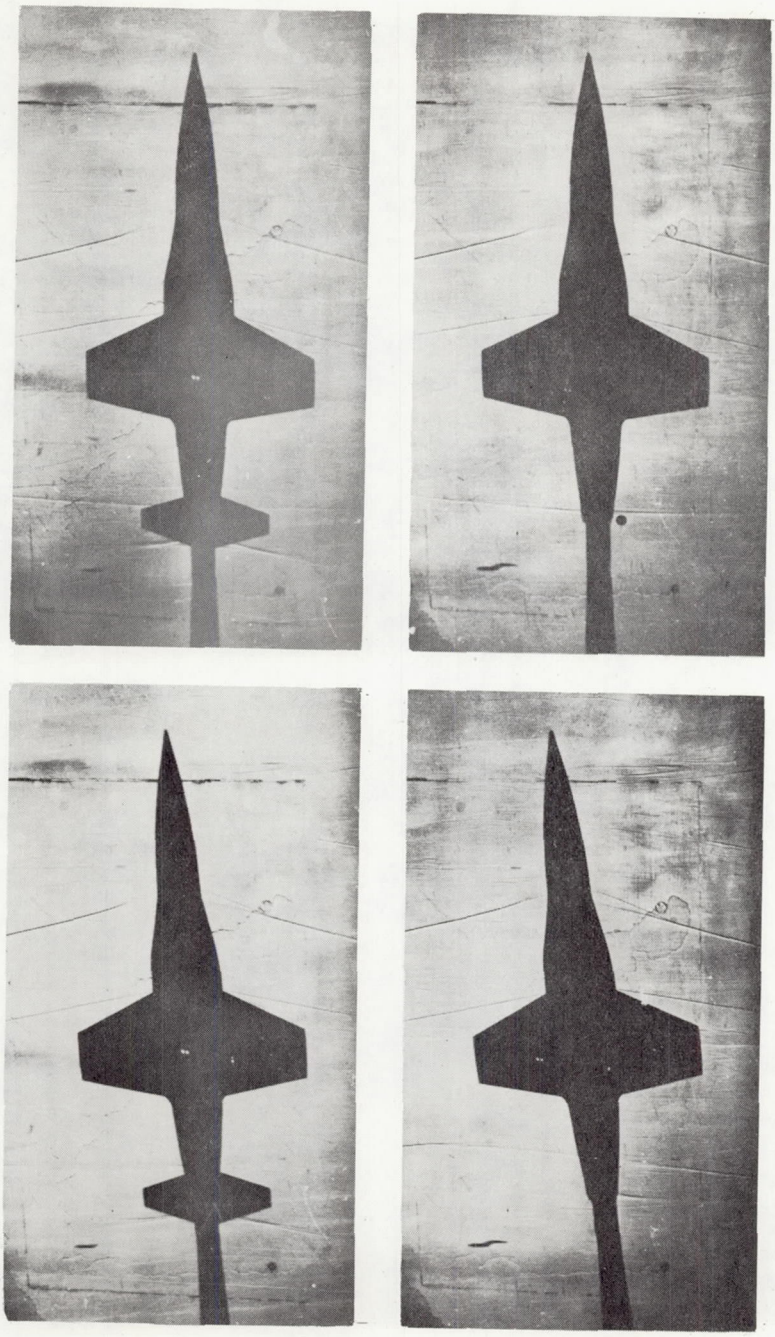

(f) M = 1.00. L-89364

Figure 14.- Continued.

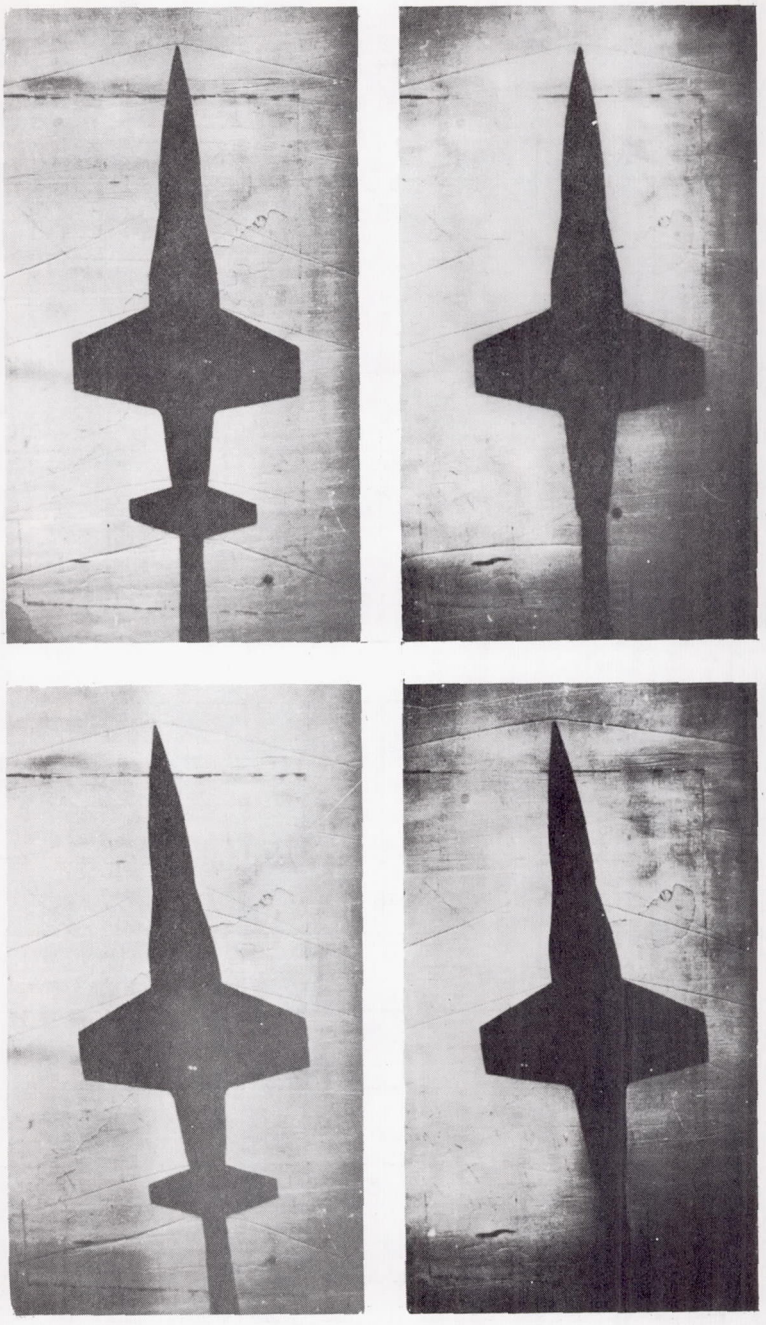

(g) M = 1.06. L-89365

Figure 14.- Concluded.

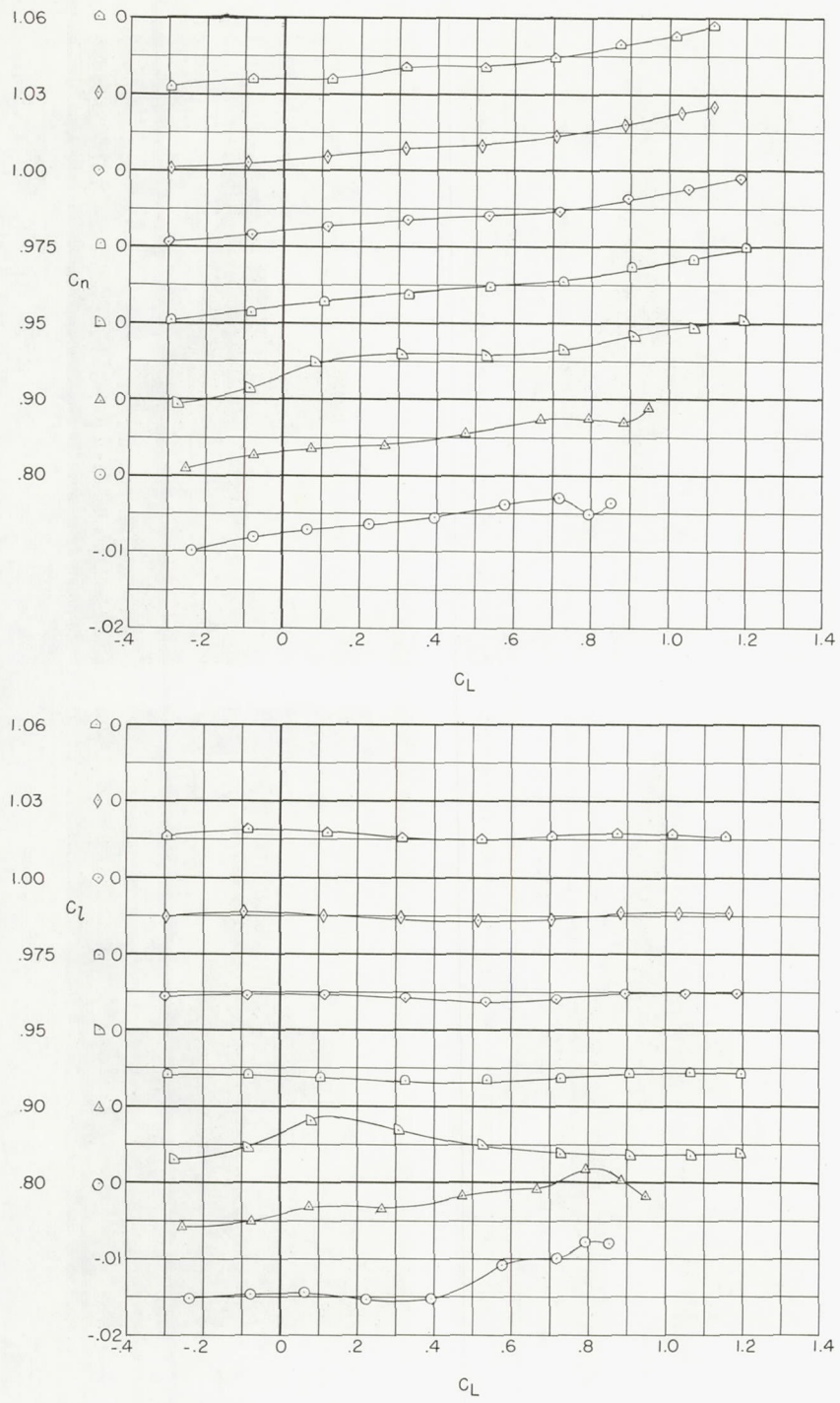

(a) a_{L-20}, complete model.

Figure 15.- Variation with lift coefficient of the lateral characteristics for several aileron deflections.

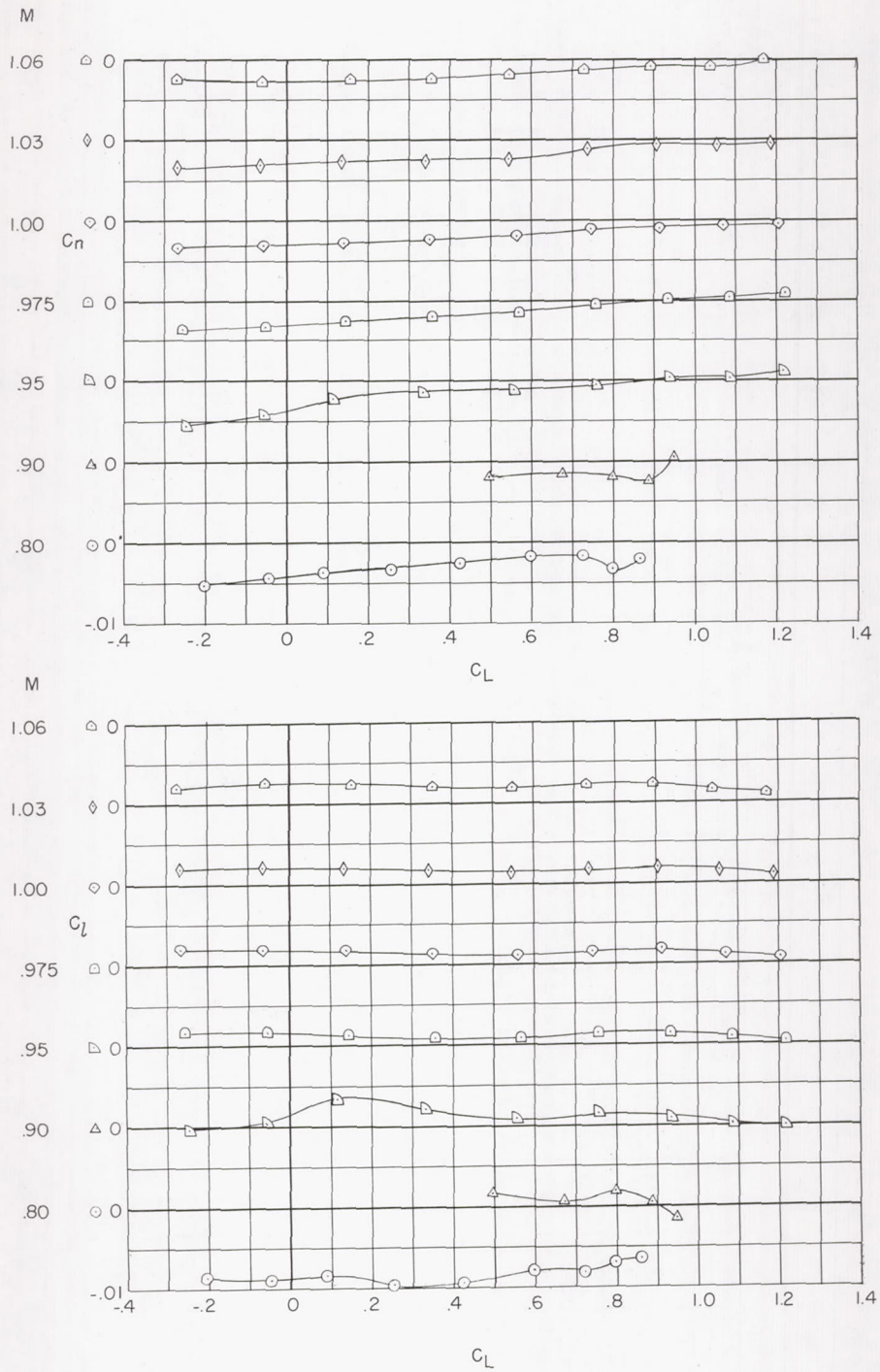

(b) a_{L-10}, complete model.

Figure 15.- Continued.

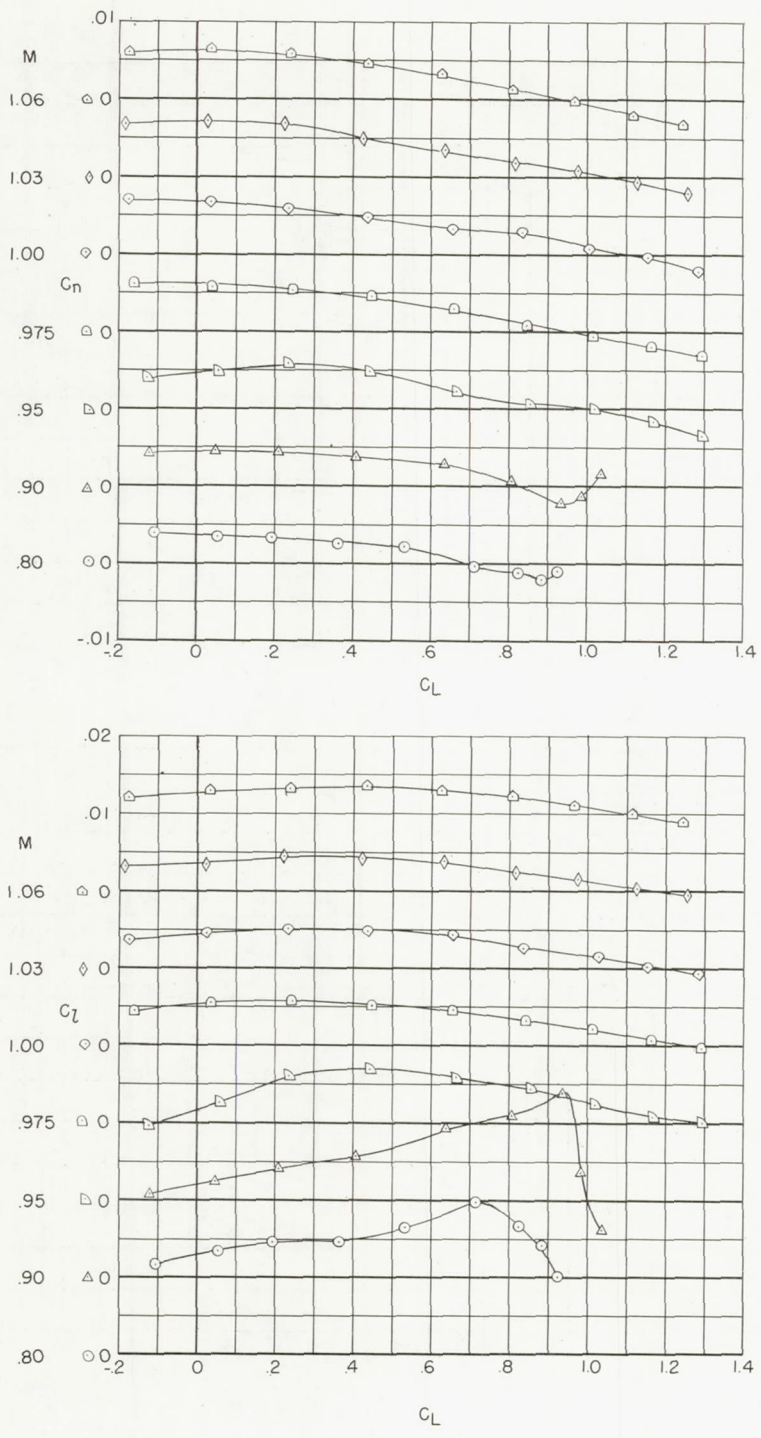

(c) a_{L+20}, complete model.

Figure 15.- Continued.

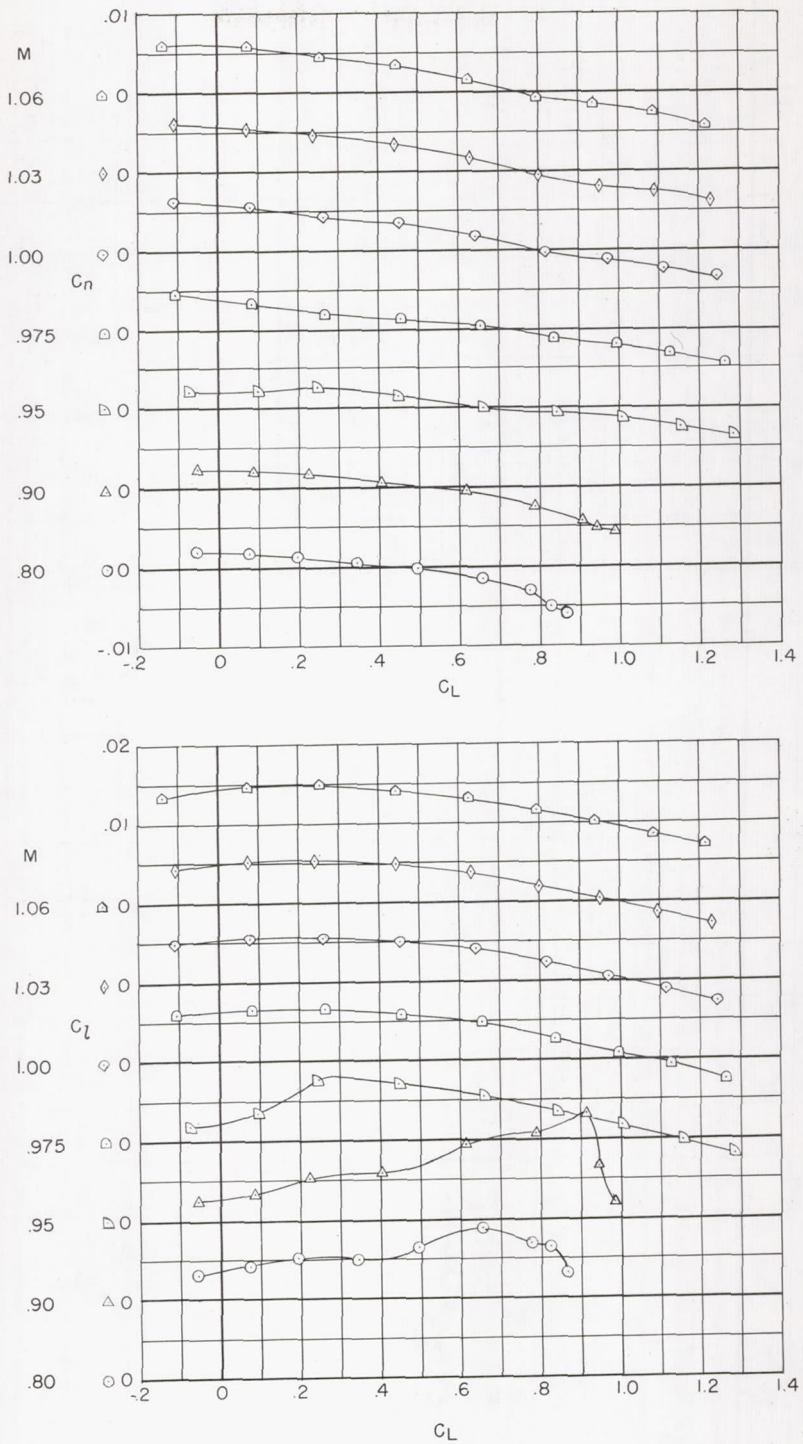

(d) a_{L+20}, horizontal tail off.

Figure 15.- Continued.

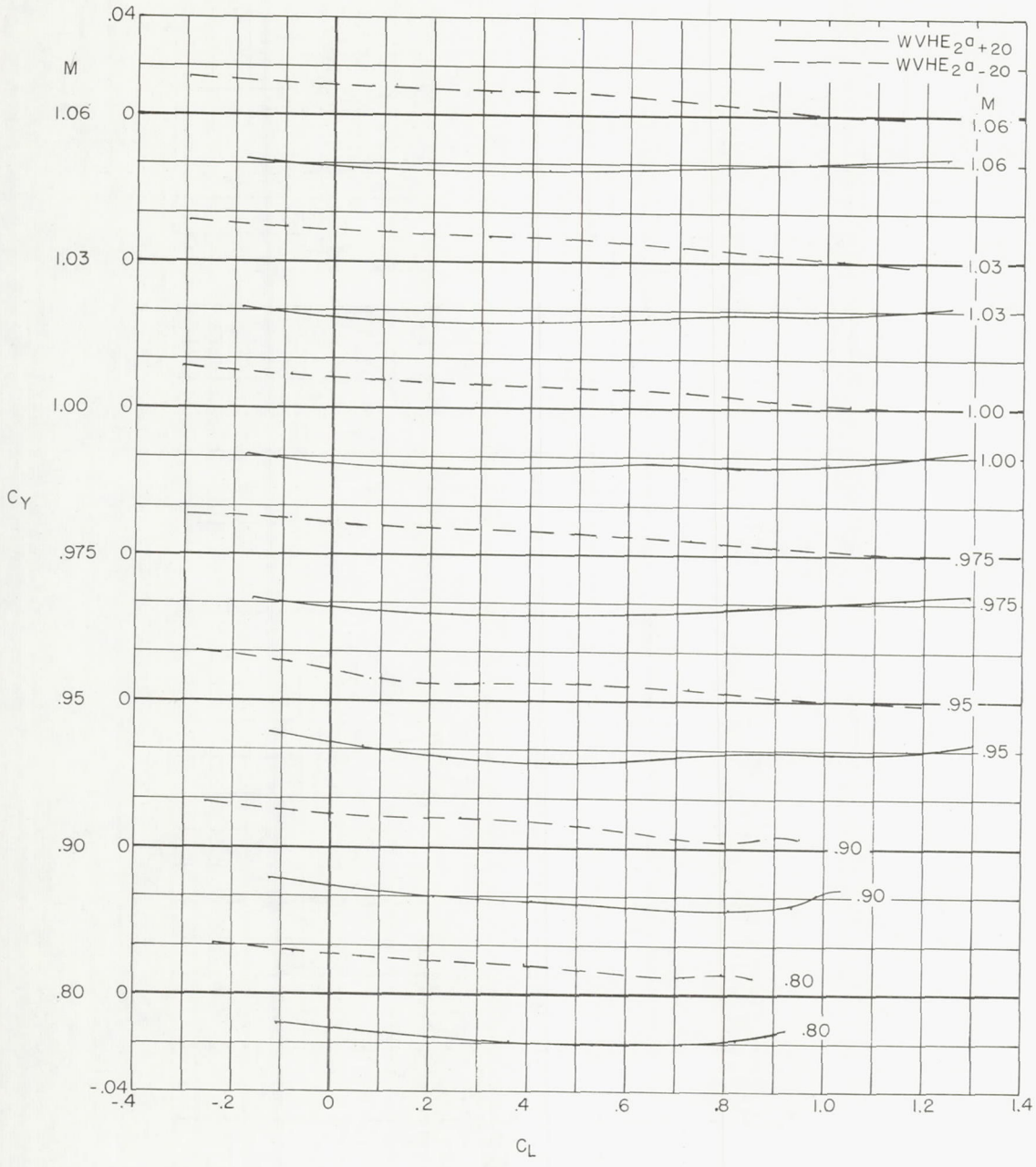

(e) C_Y against C_L.

Figure 15.- Concluded.

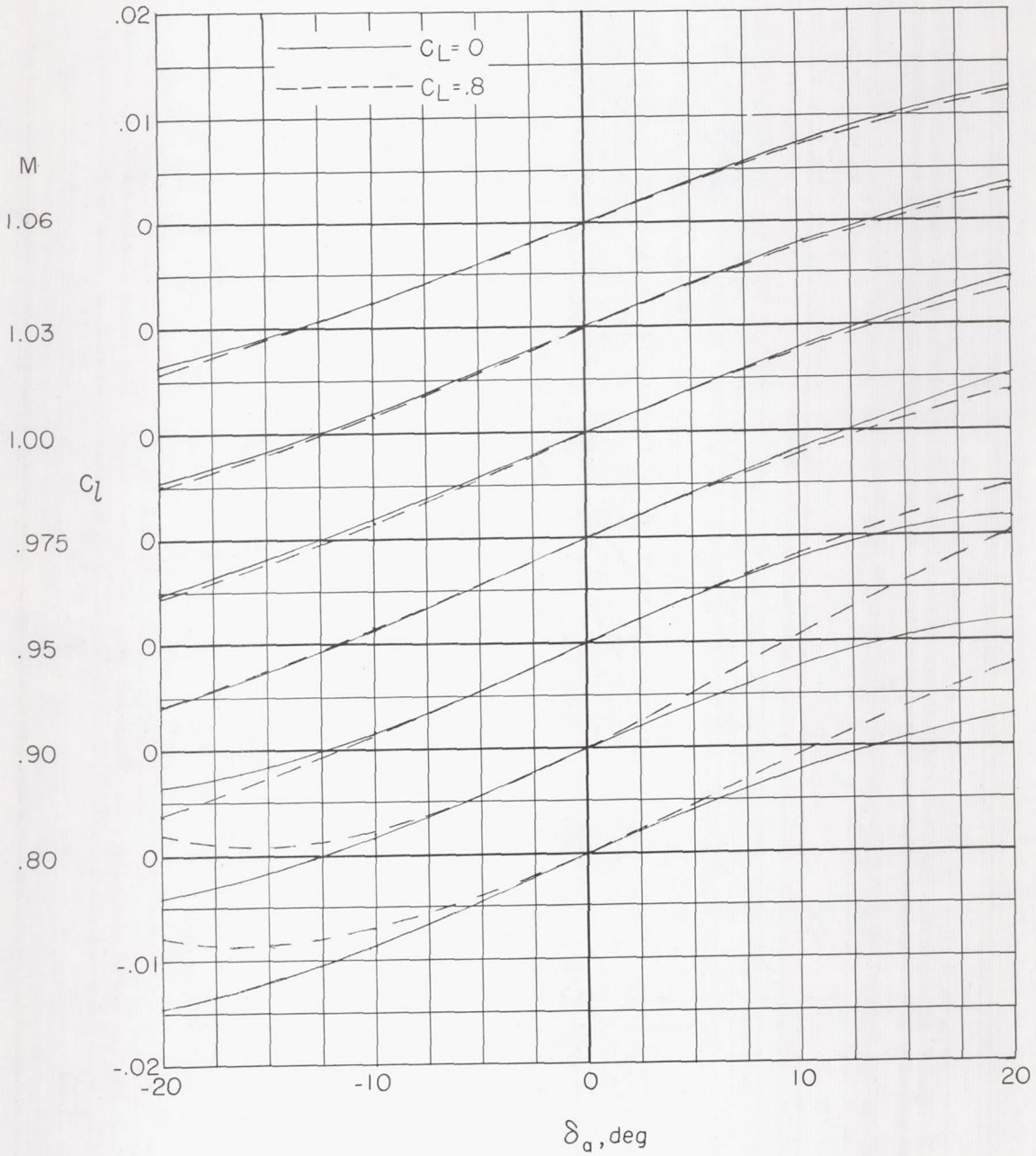

Figure 16.- Variation of rolling-moment coefficient with left aileron deflection. Complete model.

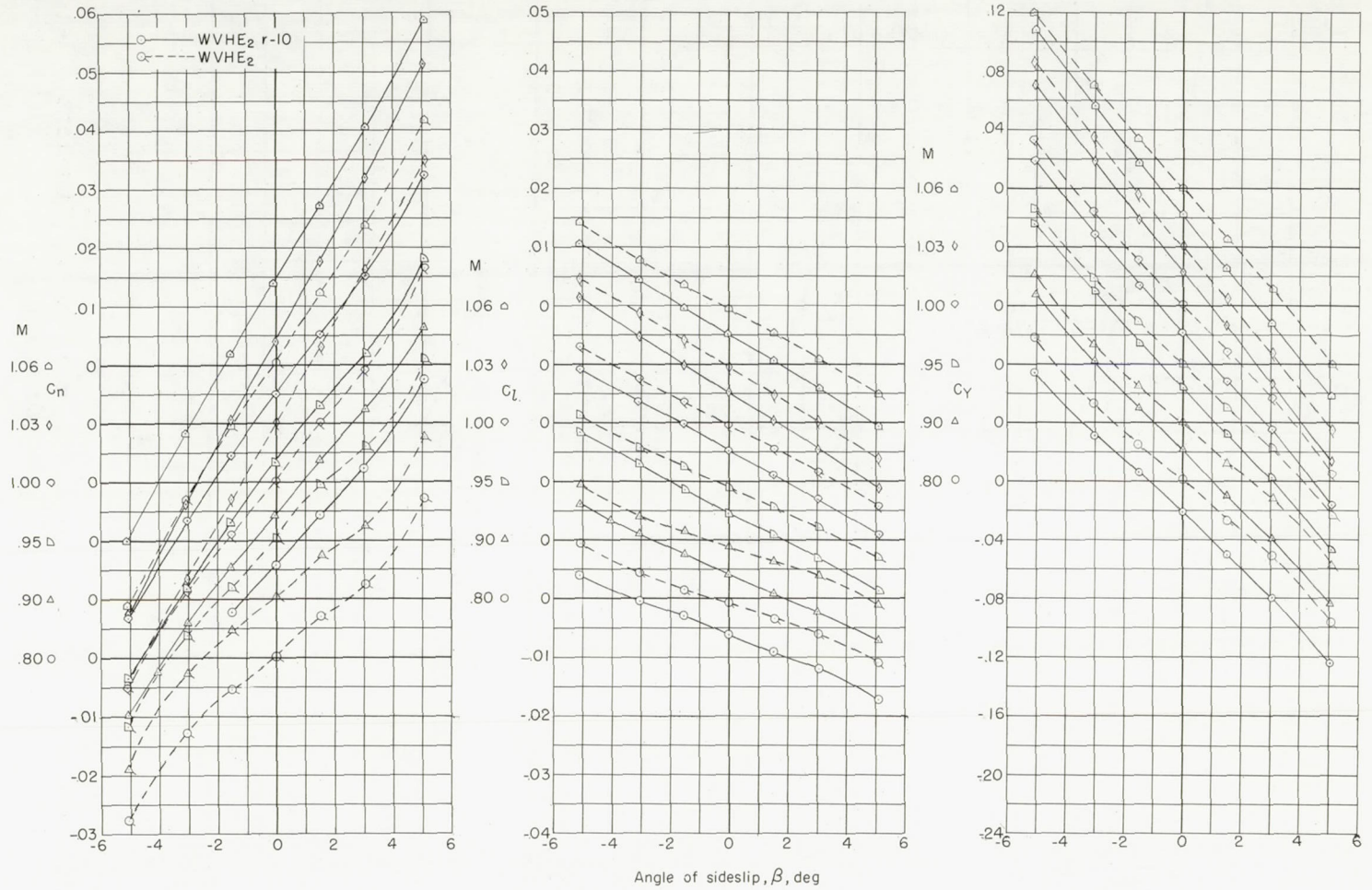

(a) Rudder.

Figure 17.- Effect of rudder and yaw damper on the lateral characteristics of the model. $\alpha = 0^{\circ}$.

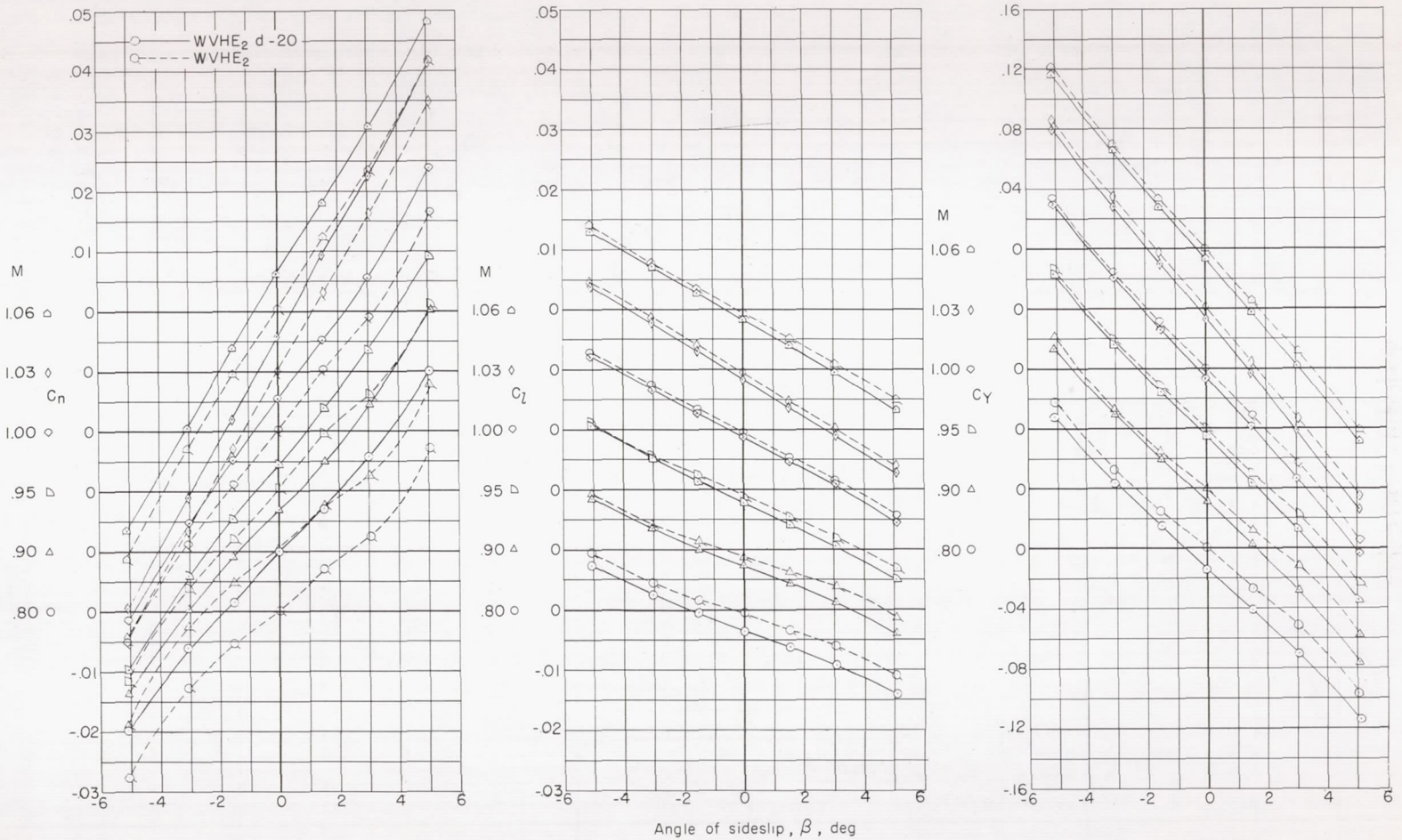

(b) Yaw damper.

Figure 17.- Concluded.

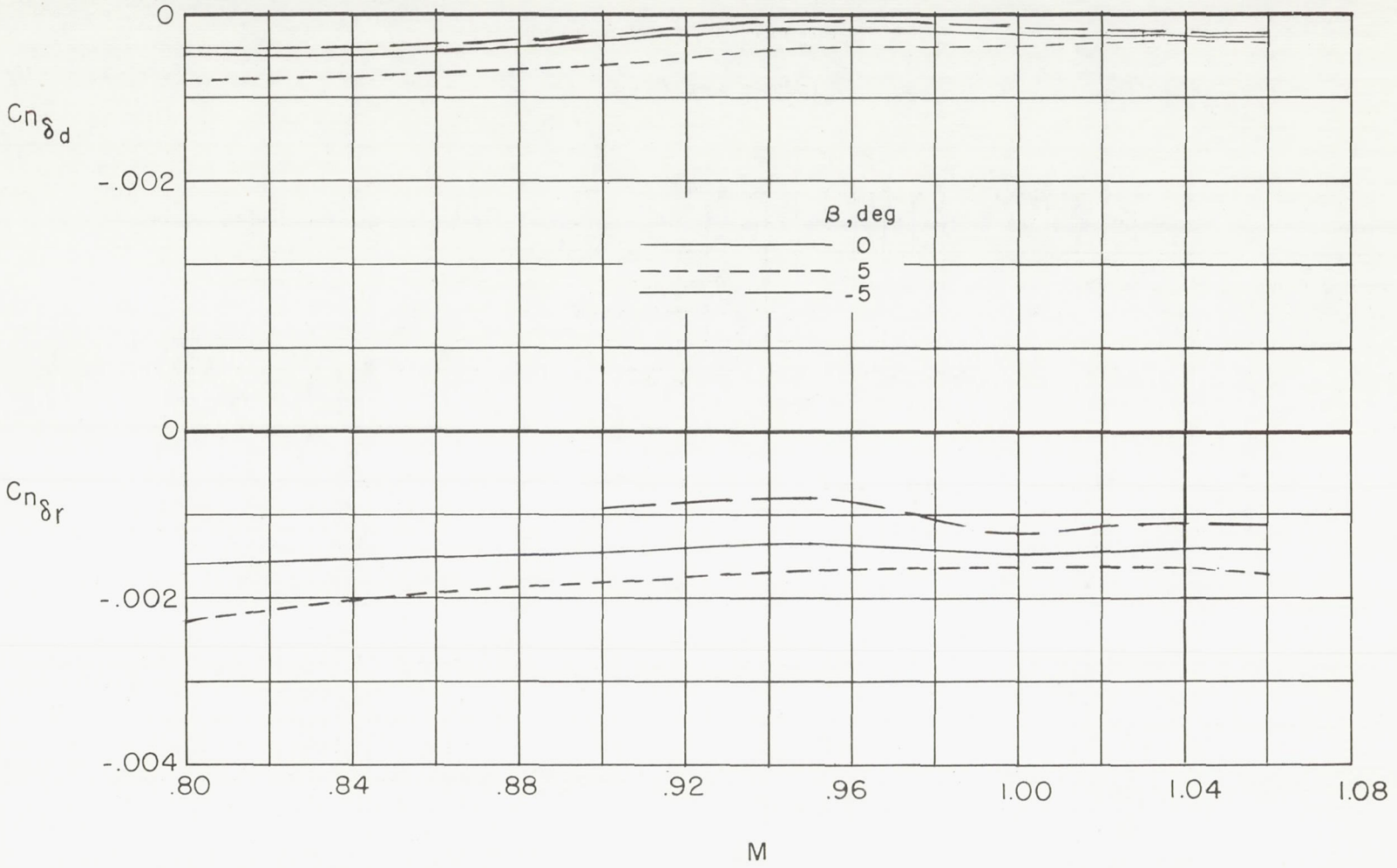

Figure 18.- Variation with Mach number of the rudder and yaw damper effectiveness parameters.